# Water balance-based approach to improve understanding of Drought Development

## by calculating the root storage deficit


By

Piet Storm


in partial fulfilment of the requirements for the degree of

**Master of Engineering**
in Water Management

at the Delft University of Technology,
to be defended publicly on Tuesday January 31, 2022 at 10:00 AM.


Supervisor: Ruud van der Ent
Thesis committee: Miriam Coenders, Riccardo Taormina


TU Delft

# Contents

# LIST OF FIGURES

## LIST OF TABLES

# Abstract

This work provides a water balance-based approach to improve understanding of drought trends by calculating root storage deficits in the United States. To do this, data is ultimately compiled from 1125 watersheds for the years 2001 to 2016. The root storage deficit is then determined using iteratively optimized transpiration values minus the water available to plants and compared to the latent heat of the FLUXCOM energy fluxes data. The stimulus for this work is a better understanding of desiccation processes. Answers to this are given only indirectly. For example, no concrete consequences can be derived from the calculated root storage deficits. Furthermore, it turns out that the water cycle-based approach provides clearly interpretable results only for catchments with sufficient water supply. Thus, increasingly arid catchments do not satisfy the general conditions required for the calculations. Catchments in which the root storage deficit exceeds one meter are declared as ever-growing deficit. In these catchments an increased drying process is to be assumed. In all other catchments, temporally congruent developments are shown for both applied methods. Due to the increased dependence on incoming precipitation, calculations performed with the CHIRPS dataset were repeated with the CRUNCEP dataset. This turns out to be generally smaller but confirms the drying processes suggested by the CHIRPS dataset. In contrast, the extents of drying suggested for both methods differ by up to 972 mm for the CHIRPS precipitation dataset, with holistically calculated root storage deficit maxima differing by an average of 178mm. This work is nonetheless useful because otherwise only grid dataset-based and thus statistically adjusted approaches are common in climatological science. Thus, the water cycle-based approach provides a concrete application of the raster values to point measurements.

# 1. Introduction

In this article, specific impacts of drought in river basins in the USA are calculated, taking into account the hydrological cycle. The impacts are determined by the so-called Discharge Method and compared with impacts based on machine-learning data sets. Specifically the FLUXCOM energy fluxes product data sets were used. In addition, the background of the FLUXCOM project and the raw data and measurement methods underlying this data set are explained. The discrepancies between hydrologically calculated parameters and concrete impacts on ecosystems mentioned in Streudle (2000) are also explained in more detail. Additional information on the FLUXCOM RS+METEO product is provided in Chapter 2. Evaporation is an essential component of the hydrological cycle. It is composed of the energy boundary (formed by solar radiation) and the availability of water. This is also known as the water boundary. Evaporation, which is determined by the energy limit alone, is also called potential evaporation. As mentioned, this consists only of energy supply and can therefore be determined relatively easily from the incident angle of the solar radiation (Coenders, 2017). For the calculation of actual evaporation, there are many more factors involved, making it much more difficult to correctly predict the latent heat of evaporation. Understanding evaporation is central to a better understanding of the global water cycle (Brenner, 2021). In practice, it is evident that the determined values of evaporative fluxes from different measurement methods often differ. Even if these methods have their justification in detail, it is not possible to give a blanket answer where and under which conditions the individual methods perform best. Basically, two approaches to measuring evaporation can be identified:

### Eddy covariance data

Eddy covariance measurement sites use in-situ measurements of vertical airflow to determine parameters for determining local evaporation. Both the turbulent fluxes of sensible heat and latent heat are determined. It should be noted that evaporation originates from latent heat. In addition, variations in wind components, temperature, and absolute humidity are measured. Eddy covariance measurements are considered a direct and reliable method for performing long-term measurements. In the FLUXCOM Energy FLUXES product, the FLUXNET data set is used. The FLUXNET dataset is based on 227 global eddy covariance measurement locations which are combined into one dataset. The energy corrections proposed as part of the FLUXCOM initiative (discussed in more detail in Section 2.2.1) are applied to the same FLUXNET eddy covariance measurements to compensate for inconsistencies with the remote sensing data.

### Remote sensing data

Remote sensing involves projecting sound signals or electromagnetic waves onto the Earth to make inferences about water availability based on its reflections. In addition, the net total radiation can be derived from the measured energy reflection. It should be noted that in addition to the different local measurement methods, remote sensing results can also provide evaporation results that differ from each other. The added value of the FLUXCOM RS+METEO energy flux dataset is not least the combination of the measurement methods just mentioned. The aim of the machine learning based approach is to provide additional weightings and adjustments so that the FLUXNET network of eddy covariance towers can be determined even where no in-situ measurements are available.

## 1.1. Problem definition and Research Questions

In this paper, the numerical methods of root storage deficit calculation mentioned in van Oorschott (2021) are applied to river basins in the United States. Results from the Discharge method are compared with results from the FLUXCOM method. The Discharge method is an iterative procedure for calculating transpiration while also taking in to consideration the hydrological cycle. The FLUXCOM method uses latent heat values from the FLUXCOM RS METEO Energy Fluxes product, based on the CRUNCEP precipitation dataset. These are considered equivalent to actual evaporation to determine alternative daily values of transpiration minus interception evaporation. Interception evaporation is all partial products of evaporation except transpiration. Interception evaporation results from the capacity of the interception reservoir, for more details see chapter 4. The resulting transpiration daily values are later used to determine the water balance of plants in the catchment areas. Periods of time when more water is removed from plants than is added are defined as root storage deficits. As described in Wang-Erlandsson (2016) and van Oorschott (2021), this deficit allows conclusions to be drawn about the formation of roots. Thus, root storage deficit serves as a proxy of plant water deficiency and for determining drought conditions and their severity. As described in van Oorschot (2021), there are numerical approaches to root storage deficit calculation. These show that consideration of the water cycle allows representative transpiration day values to be determined. These show that in the summer of a year a deficit is created in the roots, which can usually be replenished in the more temperate period. Here, the maximum value of the temporary deficit is used to determine the extent of drought for the selected period. Thus, the root storage deficit serves to determine the extent of drought and its timing.

### Methodological framework

1125 river basins in the USA were selected as the study area, which, due to the uniform measurement procedures, represent the largest possible study area and allow statistical conclusions to be drawn about the development of drought. Not only the holistic maximum extent of drought is extracted but also the respective annual maxima and the day of occurrence. As explained in Section 2.2.5, the FLUXCOM authors compared their results with the state of the art estimates and literature. The goal of the present work is to continue the validation process of the FLUXCOM authors. For this purpose, the maxima of the root storage deficit calculated using the

Discharge method are examined with those of the FLUXCOM product for possible inconsistencies. Areas with a negative net water balance may later allow conclusions to be drawn about the overall evapotranspiration performance of the respective river basins (Sung, 2017). In statistical data analysis, especially in hydrology, the time scales of different hydrological processes differ due to the irregularity of meteorological events. For this reason, recurrent processes in the hydrological cycle can only be determined if sufficiently long time periods are considered. Thus, the years 2001 to 2016 were chosen as the time range. In this period of 16 years, it can be assumed that limited informational value does not occur (Klingel, 2015). The root storage capacity is based on the portion of the water cycle that is available to plants alone. This is additionally linked to local transpiration, which can deviate strongly from effective evapotranspiration, especially during dry periods (Nijzink, 2016). The approach to calculating root storage deficit is based on the hypothesis that plants expand their roots only when necessary, i.e. during periods of water shortage, also known as drought stress. Under this assumption, the extent of drought can be determined by the change in root storage capacity. As described in Wang-Erlandsson (2016), root zone storage capacity is the product of plant-available soil water and rooting depth. As plant available water varies seasonally, the storage capacity of the root zone also varies. Combined with the hypothesis that plants do not root deeper than necessary, it follows that plants expand their root zone when plant-available soil water decreases and becomes insufficient for supply. The lack of water is therefore primarily responsible for the development of the root zone. In order to obtain concrete values of root storage deficit, van Oorschott (2021) applied methods to calculate root storage capacity using local runoff, which is why this method is used as the Discharge Method in this work. The goal underlying the further consideration of this paper is:

*If the Discharge method is applied in sufficient river basins in the USA and compared with results of the FLUXCOM energy fluxes product on the status of the root storage deficit, statements can be made regarding the applicability of the Discharge method and its results on the formation of roots.*

It can be concluded later that the storage capacity of the root zone provides information about spatially varying changes in the hydrological characteristics of an area and can therefore be useful to detect changing hydrological conditions (de Boer-Euser,2016). As described in Liu (2015), current techniques for detecting drought developments towards desertification, whether based on raster maps or field measurements, are insufficiently studied scientifically. Thus, no conclusion can be derived regarding the specific consequences with respect to fluctuations in the water cycle. A clear link is obvious but these concepts must still be considered in a differentiated way. Comparison of the two resulting root storage capacity trends will show whether the FLUXCOM energy dataset is generally suitable to provide corresponding insights. Runoff data and their catchments were requested from the USGS. In order to obtain catchment-specific representative values, only raster-based data is used, apart from the measuring points of the local runoff, and for each catchment area the respective area shares of the raster values are weighted according to the resolution of the data set. Thus, the following raster data sets are used for the following processing. For precipitation, the CHIRPS dataset is used. To obtain potential evapotranspiration data, the $E_{pot}$ product of the GLEAM dataset is used. Data of latent heat are used from the FLUXCOM Energy fluxes product. For the most comprehensive analysis possible, only the most promising approach, i.e. the latent heat results in RS + METEO, is used. The raw data and analysis methods used for this purpose are explained in more detail in chapter 3.1.

# 2. Theoretical Framework

In the following chapter, the background of machine learning in the FLUXCOM ensembling is explained in more detail. In addition to the general methodology, the most promising products for my analysis will be differentiated and synthesized. There are several approaches to match remote sensing data and steady-state measurement results using machine learning the FLUXCOM initiative of the University of Jena. It contains not only global evapotranspiration data but also climatological and hydrological parameters, which are usually matched with eddy co-variance measurement points and therefore have a wide range of parameters. In the following, the approach "The FLUXCOM ensemble of global land-atmosphere energy fluxes", is pursued in more detail.

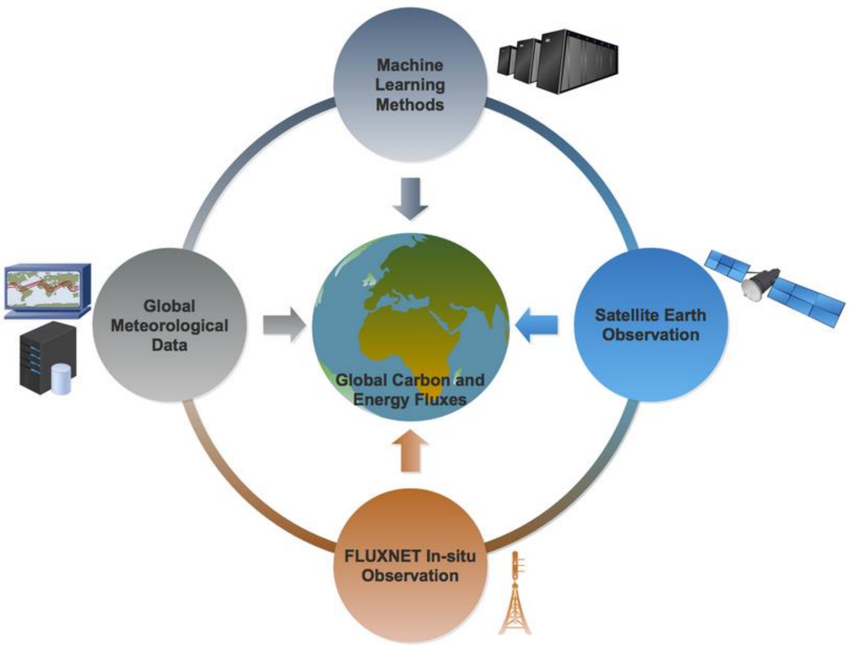


Figure 1: A general overview of the FLUXCOM initiative (Jung, 2019)

The aim of the FLUXCOM initiative is to complete the existing network of in situ measurements of the FLUXNET initiative, using FLUXNET observations and adding them together with satellite data and global meteorological data to a machine learning approach which is schematically illustrated in Figure 1. Effectively, the FLUXNET network is extended by its missing measurement points.

## 2.1. FLUXCOM basics

FLUXCOM is a 2018 project that combines energy flux measurements from FLUXNET monitoring sites with remote sensing and meteorological data using machine learning. This allows the creation of a global evaporation data estimate available at 0,5° resolution (Jung, 2019). The products of the FLUXCOM initiative consist of an approach based on remote sensing data alone, and a second one in which meteorological data have been added to the machine learning algorithm as well. The data sets based on remote sensing data alone are neglected in this work due to the higher reliability of data supported by meteorological data. The FLUXCOM energy fluxes dataset represents a combination of the results of the FLUXNET eddy covariance towers, as well as the remote sensing and meteorological data. The energy fluxes determined in this way consist of the net total radiation and the corresponding division into sensible and latent heat. The latent heat can later be added one-to-one to the estimated actual evaporation. The following data and measurement methods were used as a basis for the FLUXCOM procedure and have been assigned to clarify the aim of the later applied value tables:

#### RS: Moderate Resolution Imaging Spectroradiometer (MODIS) satellite data.

Includes land cover data from 2001-2010 and is taken without consideration of possible land cover changes. Includes daytime and nighttime land surface temperature, land cover, and fraction of photosynthetically active radiation absorbed by a canopy (Ryu, 2001). From the MODIS land cover data, which are available in three spatial resolutions (250m, 500m, and 1000m), a 0,5° raster of representative plant functional types was created by linear interpolation of 8-day values (Jung, 2019), (NASA,2014).

#### EC - Measurement dataset - FLUXNET

The FLUXNET2015 dataset is a global initiative to provide CO2 water and energy fluxes derived from eddy covariance measurements (Pastorello, 2015). For this purpose, 212 measurement sites are available worldwide. Based on the data collected there, a global map is created that indicates net ecosystem exchange (NEE), ecological respiration (RECO) and gross primary production (GPP). The measurement period is more than 20 years and is monitored and analysed by the AmeriFLux Management Project (AMP) and the European Fluxes database, as well as the ICOS Ecosystem Thematic Centre (ICOS-ETC) (Pastorello, 2015). Data processing consists of data quality assurance and quality control.

### CRUNCEP

The CRUNCEP dataset is an atmospheric climate forcing dataset used as input to land surface models. In particular, this dataset is intended to drive the Community Land Model over a long time period. The CRUNCEP dataset represents a combination of two existing datasets, the CRU TS3.2 0,5 x 0,5 ° monthly data covering the period from 1901 to 2002, and the NCEP 6-hourly 2,5 x 2,5 ° reanalysis data covering the period from 1948 to 2016 (Viovy., 2018).

### GLEAM

The Global Land Evaporation Amsterdam Model (GLEAM) is an assemblage of algorithms which evapotranspiration based on a Priestley-Taylor formulation with explicit soil moisture stress, and interception by the GashModel43, and was informed by various satellite forcing data (Jung, 2019) (Martens, 2017). Since the GLEAM dataset contains a large amount of data, it should be noted that the evapotranspiration dataset (v3.1a) was used for the cross-consistency check of the FLUXCOM initiative. The extension of the cross-consistency check carried out in the paper is based on the potential evaporation $Epot$ (mm/d) and is taken from a later publication version of the GLEAM dataset (v3.3).

### LandFLux-EVAL

LandFlux-EVAL is the ensemble mean of evapotranspiration products based on different approaches. For the net radiation Rn, two satellite-based products from Clouds and the Earth's Radiant Energy System are compared with each other to obtain corroborated values of net radiation (CERES, 2021).

## 2.2. Machine Learning FLUXCOM

In this chapter the overall methodology of the FLUXCOM global land-atmosphere energy fluxes is explained in more detail. Note that due to the consideration of climate data only the RS+METEO approach is discussed. The machine learning approach in the FLUXCOM project is used to obtain a prediction for the latent heat and the sensible heat. The applied algorithms are applied to the FLUXNET in situ measurements to fill in the missing measurement points.

### 2.2.1. Preparation of dependant variables

Before the FLUXNET data is presented to the algorithm for training, an energy closure adjustment is made. These adjustments follow 3 different approaches". The general form of the correction is $x_{LE} * LE + x_H * H = R_n - G$ , where G is the ground heat flux, and$x_{LE}$ and $x_H$ are the correction factors for latent and sensible heat, respectively". (Jung, 2019). The authors assume that the bowen-ratio optimisation, which assumes that the ratio of sensible heat to latent heat is accurately measured and both receive the same correction factor: $x_{LE+H} = x_{LE} = x_H$ To force the energy balance closure,$x_{LE} = \frac{(R_n-G)}{(LE+H)}$ . In the residual approach, the missing energy is then attributed to either $H$ ($H_{res}$) or $LE$ ($LE_{res}$). $LE_{res}$ with $x_{LE} = \frac{(R_n-G-H)}{LE}$,$x_H = 1$ and $H_{res}$ with $x_H =$

$\frac{(R_n-G-LE)}{H}, x_{LE} = 1$.The correction factors are then continuously estimated from the 30-day median. The algorithm can then recognise latent heat and sensible heat as such and only needs to be fed with sufficient independent variables.

### 2.2.2. Prediction variables

To support the algorithm with sufficient data, use is made of MODIS land products. MODIS products include daytime and nighttime land surface temperatures, land cover, the fraction of photosynthetically active radiation absorbed by a canopy, and the bidirectional reflectance distribution function (Jung, 2019). “The Land Cover Dynamics product includes layers on the timing of vegetation growth, maturity, and senescence that mark the seasonal cycles. Estimates of vegetation phenology are provided twice annually from the two 12-month focus periods, July-June, and January-December, allowing for hemispheric differences in the growing seasons, and enabling the product to capture two growth cycles if necessary.” (NASA, 2014). These data are cut to a 0,5 ° grid and tiled by plant function type. Seasonal cycles are then created by linear interpolation of 8-day values.  Four different commonly used Global climate forcing datasets are used to obtain meteorological data (CRUNCEPv8). The water availability indices were calculated for each forcing dataset based on daily precipitation and potential evaporation.

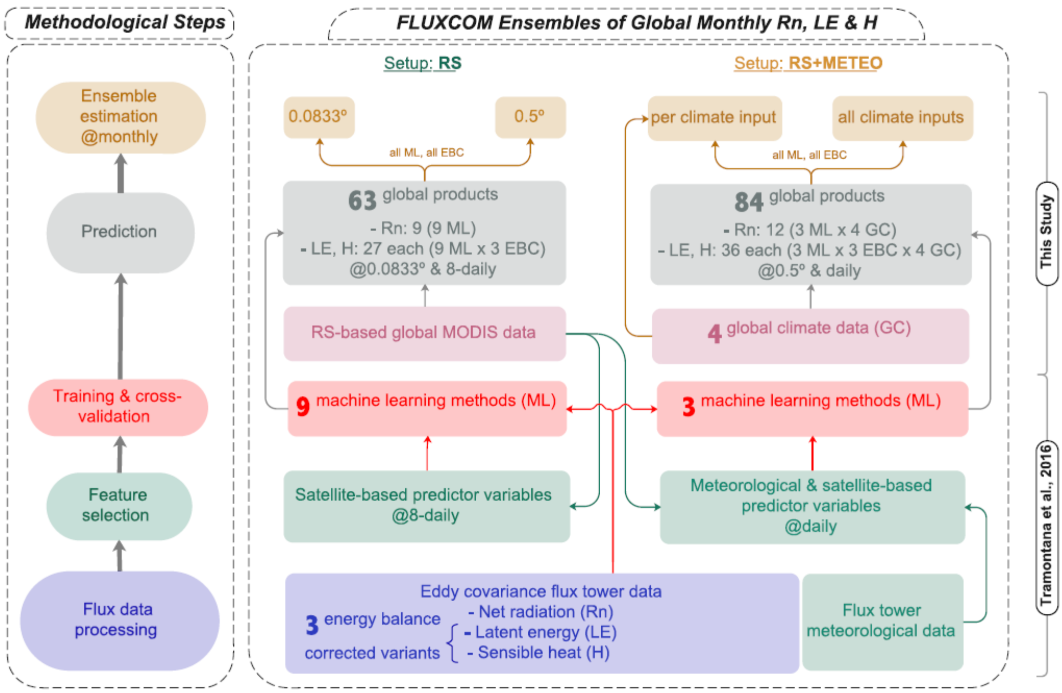


Figure 2: Illustration of methodological steps and resulting ensemble members for the RS and the RS+METEO approach according to (Jung,2019).

### 2.2.3. Predicton of LE and H

In order to obtain a representative prediction, three machine learning methods are used to predict $R_n$, $LE$ and $H$. The machine learning algorithms used for this follow the approach of convolutional neural networks. The full factorial design approach ensures that all potential sub-products are taken into account. These contain 4 different global climate data, where 3 correction factors are added for $LE$ and $H$ respectively. This results in 84 sub-products with their respective specific partial results. The methodological steps and the resulting partial products are shown in Figure 2. In the RS+METEO setup ensemble products for mean monthly fluxes are generated, where the ensemble estimate corresponds to the median of the ensemble members for each grid cell and month. For a more precise determination of the ensemble dispersion or uncertainty, the median absolute deviation is also included.

### 2.2.4. Cross-consistency checks with state-of-the-art estimates

Spatial patterns of mean annual LE and Rn fluxes and the monthly time series of their continental means from the FLUXCOM ensemble are compared with previous estimates. For LE, the FLUXCOM RS and RS + METEO ensembles are compared with the Model Tree Ensemble (MTE10), the Global Land Evaporation Amsterdam Model (GLEAM v3.1) and LandFlux-EVAL41. The MTE is based on only one machine learning method, trained on monthly flow data, and can be considered a precursor to FLUXCOM. Due to the increased data situation and the associated increased data-based security of confidential values, it was decided to use only the RS+METEO product. Since 8-day values were used instead of daily values in most of the sub-products, a subproduct was selected that provides daily values and covers as long a time span as possible in order to simplify the calculation. A maximum time span from 2001 to 2016 was determined for the CRUNCEP ensembled result. This is based on a meteorological product, the CRUNCEP precipitation data set, and is based on all 3 machine learning methods.

# 3. Applied methods

This chapter first explains the attached data and its pre-processing. Then current ambitions for calculating root storage development are presented. In this way, the FLUXCOM data are not only compared with potential evaporation in general but also in dry periods (Sung, 2017). There is thus an additional dependency on water inflow, i.e. precipitation, which is first calculated using the CHIRPS dataset and then qualitatively compared with the CRUNCEPv7 dataset. By examining FLUXCOM performance through the calculation of the root storage deficit, not only the performance in periods of drought but also the replenishment of these deficits and thus the holistic development of the respective region is taken into account. Ultimately, the respective developments of the root storage deficits are compared to see whether the changes in the RS+METEO result deviate from the original information or not.

## 3.1. Data basis

In order to be able to carry out the analysis adequately, it is of utmost importance to obtain reliable and sufficiently long data series. In addition, the measurement methods used should be as comparable as possible. Due to the large national area and the resulting uniform measurement techniques, the calculations are carried out exclusively in the USA. For this purpose, all measuring points marked as river courses and their coordinates were overlaid with the available boundary data. Last but not least, the associated data sets of local discharges had to have the time span of the FLUXCOM data, namely from 01.01.2001 to 31.12.2016. If the first calculations lead to satisfactory results, further areas can be added to the calculations. For a comprehensive analysis, these would have to be distributed as widely as possible across the globe in order to detect possible deviations in the quality of the data. Of the originally selected catchments, some may be dropped because the requested data series of local runoff are either not complete, or are based on estimated values instead of measurements. Although the available data are based on daily measurements and calculations, in this paper the results for annual and total extreme values are calculated and used as a basis for the further explanations. This makes it possible to compare potential impacts of possible dry periods across years (Wang-Erlandsson, 2016). Furthermore, conclusions can be drawn in a holistic context.

### Discharge readings

In order to be able to cover the area of the USA accordingly, the available discharge measurement values in the USA were queried. Subsequently, all areas marked by the USGS as river course and their measurement series were downloaded and their catchments marked by the USGS were displayed as polygons and assigned to the respective river catchments by triangulation. Subsequently, the Discharge related to the area of the respective catchment was used in further calculations in order to calculate consistently in mm/d.

### Potential evaporation data

For the potential evaporation data needed in the upcoming calculations, the GLEAM v3.3 dataset was used (Martens et al., 2017). This is the same dataset mentioned in Chapter 2 but it is a newer version and a different variable, namely potential evapotranspiration $E_{pot}$(mm/d). To combine point values and raster data, the raster values and their area weighting were adjusted to the catchments and a representative mean value was calculated which corresponds to the determination of representative values (Miralles, 2011).

### Precipitation data

In the present work, the decision was made not to use point measurements for precipitation but to use the CHIRPS precipitation grid. This has a lower accuracy in relation to the actual local precipitation but is more representative of the long-term total precipitation due to the statistical adjustments. The Climate Hazards Group Infrared Precipitation with Stations (CHIRPS) dataset is a combined product of remote sensing and in situ observations with high resolution (Ullah, 2019) and daily precipitation estimates based on the duration of cold clouds. In a first step, station data are blended to produce a preliminary information product. Then, a blending procedure is applied that takes into account the spatial correlation structure to assign interpolation weights (Funk, 2015). To combine point values from other data series with the raster data, the raster values and their area weighting were tailored to the catchments and a representative mean value was calculated.

### FLUXCOM latent heat Data

The latent heat data is derived from the LE.RS_METEO.EBC-ALL.MLM-ALL.METEO-CRUNCEP_v8.720_360.daily dataset. Generally, the latent heat of the FLUXCOM dataset is equated with the actual evaporation. This is not quite correct, as the actual evaporation also depends on the local temperature (Jung, 2010). However, the fluctuations in temperature are so small that this can be neglected. The resulting factor for actual evaporation is $\rho\lambda$=2.45 (GJ/$m^3$) (Coenders, 2017).

## 3.2. Discharge method for estimating root zone storage capacity

In this chapter, the previously mentioned data is processed. The respective catchment areas are first divided into two fictitious storage media. The water available to the roots is then determined in the storage medium associated with transpiration. The fluxes associated with precipitation and evaporation, also called vertical water flows, are explained in Figure 3. In order to carry out the validation especially in extreme situations, it was decided to specifically investigate droughts. According to Wang-Erlandsson (2016), the root storage capacity model is based on the observation that plants do not root deeper than necessary to meet their water needs. This means that during dry periods and at dry sites, root growth takes place to a much greater extent to reach the water-bearing layers than at moist sites with high groundwater levels. The root mass at dry sites, which can serve as a water reservoir, is correspondingly greater. This allows possible qualitative differences to the FLUXCOM evapotranspiration data set during the dry periods mentioned and the resulting variation of the root storage deficit to be identified. In this context, the daily values determined are not only examined for their informative value with regard to the long-term water cycle but specifically during dry periods. In the search for a suitable calculation method, it was decided to use the Discharge method, which has been used for some time as a tool for calculating mass shifts of fluids (Gao, 2017). This method is commonly used to determine the required storage capacity of reservoirs. It is not only a matter of the maximum filling quantity but also of the final emptying of the reservoir without overflowing.

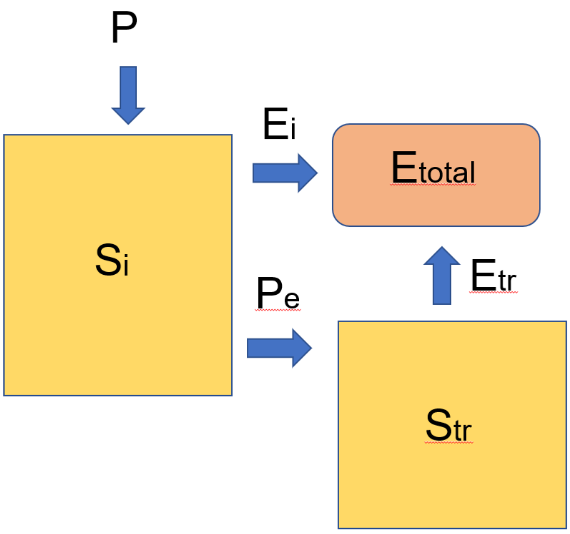


Figure 3: Explanation of the storage media used and their incoming and outgoing flows. $\boldsymbol{S_i}$ (mm) depends on the incoming rain $\boldsymbol{P}$ (mm/d), the outgoing interception evaporation $\boldsymbol{E_i}$ (mm/d) and the effective precipitation $\boldsymbol{Pe}$ (mm/d). The transpiration storage $\boldsymbol{S_{tr}}$(mm) depends only on the effective precipitation and the transpiration $\boldsymbol{E_{tr}}$ (mm/d).

As shown in Figure 3, each river basin is divided into two storage media, the interception storage Si and the transpiration storage $E_{tr}$. The interception storage represents a fictitious storage medium in which all evaporation that does not originate from plants occurs. The interception storage describes the evaporation from wet surfaces after precipitation. This includes interception from leaves as well as from wet surfaces such as vegetation, paved surfaces, fallen leaves, bare soil, etc. (Gerrits et al., 2011). Transpiration storage, on the other hand, represents the amount of water used by plants for transpiration.

The interception storage $S_i$ (mm) is thus defined as storage basin of a catchment that is responsible for all evaporation that does not take place in the form of transpiration. For both partial evapotranspiration, the assumption is that together they correspond to total evapotranspiration and actual evapotranspiration, respectively. This results in equation 1.

$$E_{total} = E_i + E_{tr} \tag{1}$$

In which the interception Evaporation $E_i$ (mm/d) is the one leaving the interception storage and the remaining transpiration $E_{tr}$ (mm/d) is leaving the transpiration Storage.

Whereby it must be further examined whether the total evaporation $E_{total}$ actually corresponds to the FLUXCOM-evaporation $\rho\lambda E_{FLUXCOM}$.

$$\frac{dS_i}{dt} = P - E_i - P_e \tag{2}$$

The change of the interception storage is determined by the incoming CHIRPS precipitation $P$ (mm/d), the outgoing interception evaporation $E_i$ (mm/d) and effective precipitation $P_e$ (mm/d). The conditions for $E_i$ and $P_e$ are indicated below.

$$\begin{array}{ll} E_i = E_{pot} & \text{if } E_{pot}dt < S_i \\ E_i = S_i & \text{if } E_{pot}dt \geq S_i \\ P_e = 0 & \text{if } S_i \leq S_{max} \\ P_e = \frac{(S_{max} - S_i)}{dt} & \text{if } S_i > S_{max} \end{array}$$

Evaporation currents cannot be greater than the energy available for it, which is defined as $E_{pot}$. Thus, the first condition is that $E_i$ is equal to $E_{pot}$ as long as $S_i$ is greater than $E_{pot}$. But if $E_{pot}$ exceeds $S_i$, $E_i$ is again bound to the capacity of $S_i$. In the second half of the conditions it is defined that as long as $S_i$ has not yet reached the maximum capacity of $S_{max}$, no $P_e$ falls. Only when $S_{max}$ is exceeded is the excess $P_e$ added. With the help of all 4 framework conditions, both a temporal offset of $P$ and $P_e$ and the consideration of the maximum evaporation Epot can be guaranteed. A maximum storage volume of $S_{max}$=3mm was set. As mentioned in van Oorschot (2021), $S_{max}$ in tropical rainforests varies between 2mm and 8mm (Herwitz, 1985). Since it is not so much the potential storage maximum that is decisive in determining the deficit but the number of days on which this occurs repeatedly, the effect of the applied $S_{max}$ is negligible. Since repeated rainy days are on average above the chosen $S_{max}$, the error due to an incorrect choice of $S_{max}$ is small. During the calculation of the interception storage, incoming and outgoing flows were compared and weighed against the current capacity of the interception storage. This allows any errors in the precipitation and potential evaporation dataset to be identified and errors in the algorithm to be detected. After the interception storage has been determined, the all-time transpiration average is determined by making use of the long-term water cycle. This is where the name of the Discharge method comes from, as it is no longer only vertical water flows that are taken into account but also horizontal water flows such as the Discharge $Q$. The perspective changes to the total area of the respective catchment areas and the discharge is now given relative to the catchment area in mm/d as in equation 3.

$$\overline{P_e} - \bar{Q} - \overline{E_{tr_a}} = 0 \tag{3}$$

Since long time arrays of $P_e$ and $Q$ are determined by applying the Discharge method and reading in USGS data the overall transpiration $\overline{E_{tr}}$ is derived from equation 3. Afterwards the whole-time transpiration coefficient (-), which is defined as the ratio of Transpiration and the total potential Evaporation derived from the GLEAM dataset is determined as stated in equation 4.

$$c_{0,a} = \frac{\overline{E_{tr_a}}}{\overline{E_{pot}}} \tag{4}$$

Here $\overline{E_{tr}}$ (mm/y) is the previously determined holistic transpiration average and $\overline{E_{pot}}$ (mm/y) is the overall potential evaporation for the period a=01.01.2001-31.12.2016. Subsequently, the first preliminary transpiration daily values are determined while assuming that the overall ratio of transpiration to potential evaporation can be equally applied on each day. The resulting equation describing the initially applied time array of transpiration is stated in equation 5.

$$E_{tr_a}(t) = c_{0,a} * E_{pot}(t) \tag{5}$$

In Wang-Erlandsson (2016), the storage capacity of the root zone is calculated using spatial precipitation and evapotranspiration datasets. This method is usually referred to as the water balance method, as it takes into account the water balance throughout the year. It is based on the basic assumption that "plants do not root deeper than necessary". The effective rooting depth is therefore directly dependent on the water surplus or deficit. This water balance was determined annually and the extreme values were noted as general maxima. An illustration of the algorithms used is given in Figure 4.

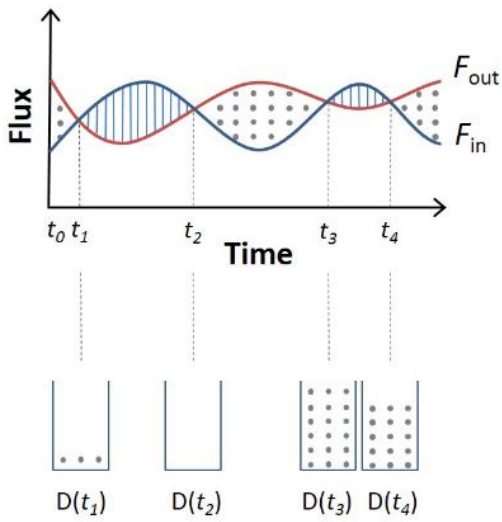


Figure 4: Illustrative representation of the algorithm calculating the root storage capacity according to (Wang-Erlandsson, 2016). As can be clearly seen in the figure, only the periods in which outgoing flows outweigh incoming flows are taken into account, resulting in a net deficit in the storage medium.

In the method described in Gao (2014) and van Oorschot (2020), the root storage deficit is calculated by determining an interception storage and a transpiration storage. The storage deficit is then calculated using the effective precipitation and the provisionally calculated transpiration as stated in equation 6.

$$S_{tr}d_0(t_0, t_1) = \max\left(0, -\int_{t_0}^{t_1}\left(P_e(t) - E_{tr_a}(t)\right)dt\right) \tag{6}$$

Here, t0 corresponds to 1 January of a year and t1 to 31 December of the same year.

Afterwards the relative change in storage deficit $S_{tr}d_0(t)$ (mm) is determined as stated in equation 7.

$$\frac{dS_{tr_{i,a}}(t)}{dt} = S_{tr}d_i(t_0, t_0) - S_{tr}d_i(t_0, t_1) \tag{7}$$

This change is then re applied into the annual water balance. Making use of the formerly used postulate that the water balance is closed the resulting mean annual Transpiration $\overline{ETr_a}$ (mm/year) is calculated.

$$\overline{E_{tr}}_i = \overline{P}_{e_a} - \overline{Q}_a - \frac{dS_{tr_{i,a}}(t)}{dt} \tag{8}$$

Subsequently, the annual transpiration is then used to calculate daily transpiration arrays as indicated in equation 9.

$$c_{i,a} = \frac{\overline{E_{tr_i}}}{\overline{E_{pot_i}}} \tag{9}$$

$$E_{tr_i}(t) = c_{i,a} * E_{pot}(t) \tag{10}$$

With the now annually determined transpiration coefficient $c_{i,a}$ (-) is calculated for each of the 16 years.

$$S_{tr}d_i(t_0, t_1) = \max\left(0, -\int_{t_0}^{t_1}\left(P_e(t) - E_{tr_i}(t)\right)dt\right) \tag{11}$$

$$S_{tr}d_{i+1}(t_0, t_1) = \frac{S_{tr}d_i(t_0,t_1) + S_{tr}d_{i-1}(t_0,t_1)}{2} \quad \text{for } i > 1 \tag{12}$$

The optimisation process from the first iteration upwards is shown in equation 12. This process is iteratively repeated until the absolute change in the transpiration coefficient compared to that of the previous iteration did not exceed the absolute threshold of 0,002.

$$0{,}75 * c_{0,a} \leq c_{i,a} \leq 1{,}25 * c_{0,a} \tag{13}$$

In order not to violate the framework condition of an intact water balance, as stated in equation 13 the change in the transpiration coefficient is allowed to deviate by a maximum of 25% from the original all-time estimate. This way the uncertainties from the water cycle are diminished in a deterministic way. Since in some catchments the threshold is not reached an additional constraint of a maximum number of 20 iterations is set.

## 3.3. FLUXCOM approach root storage capacity

In order to carry out the final evaluation of the latent heat of the FLUXCOM approach, it was first postulated to be equivalent to the actual evaporation (mm/d). Consequently, the FLUXCOM transpiration $Etr_{FLUXCOM}$ (mm/d) is directly dependent on the FLUXCOM evaporation and the interception evaporation $E_i$ (mm/d) calculated in 3.2 as given in equation 14.

$$E_{tr_{FLUXCOM}} = \rho\lambda E_{FLUXCOM} - E_i \tag{14}$$

With $\rho\lambda = 2{,}45 GJ/m^3$(Coenders, 2017). As executed in 3.1, the root storage deficit is calculated by making use if the FLUXCOM transpiration $Etr_{FLUXCOM}$.

$$S_{tr}d_{FL}(t_0, t_1) = \max\left(0, -\int_{t_0}^{t_1}\left(P_e(t) - E_{tr_{FLUXCOM}}(t)\right)dt)\right) \tag{15}$$

Whereby the iterative approach for calculating the actual transpiration is omitted.

# 4. Results

## 4.1. Individual results per catchment

In this chapter, the calculation results of the steps explained in Chapter 3 are presented and explained. First, the development of the root storage deficit is calculated with the Discharge method and then with the FLUXCOM method. It is important to note in which areas sufficient runoff data were not available and in which catchments the required conditions were not met. Figure 5 provides an overview of the suitability of the available data set as a basis for the subsequent calculation steps. As can be seen, there are catchments where the boundary conditions are met and catchments where the available discharge values are insufficient because some values were either not available or estimated instead of measured. Catchments where the boundary conditions are not met are those where the water balance is already closed without transpiration and therefore the water balance approach cannot be performed. As shown in Table 1, 7 catchments were selected to reflect the full range of results.

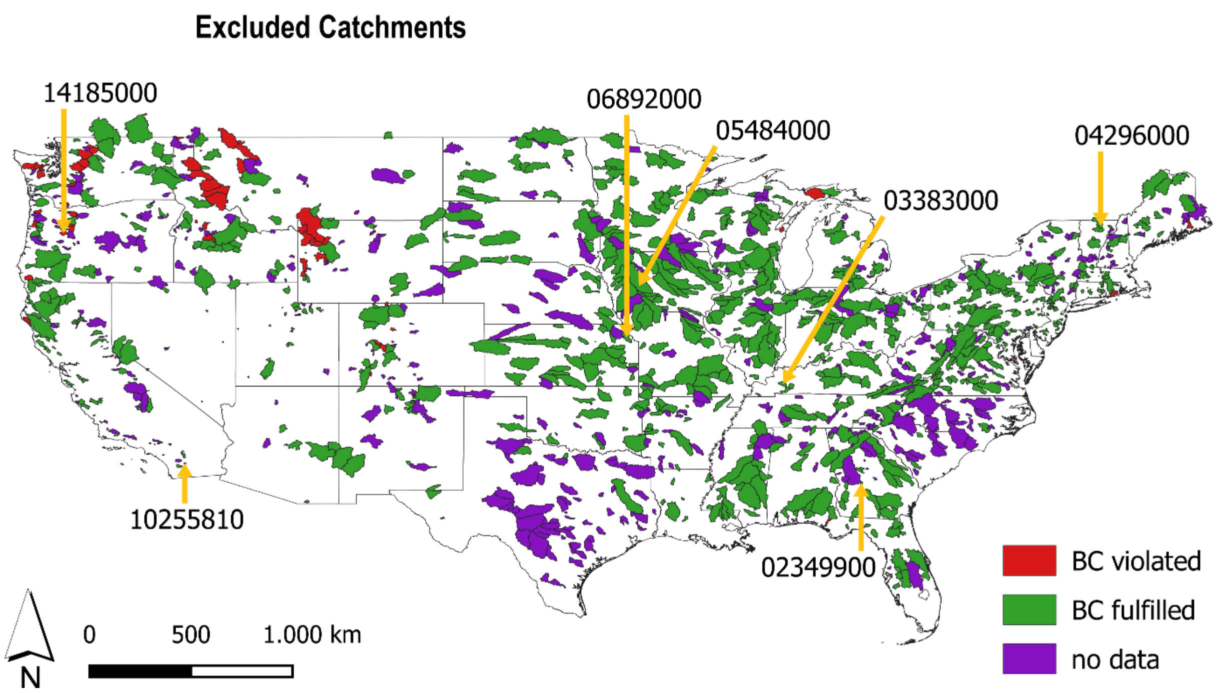


Figure 5: Presentation of the catchment areas and suitability of the data set as a basis for the subsequent calculation steps.

As shown in Figure 5, there is no clear picture of data availability. Shown in purple are catchments for which time series from January 1, 2001 to December 31, 2016 were not available or were partially estimated. The catchments where the framework is violated are only found in the north and northwest but not in the southeast.

Table 1: Example selected catchments indicated with a yellow arrow in Figure 5. They are selected to represent both expected and unexpected outcomes, including catchments where boundary conditions are violated.

| Catchment | Site number | Station name |
|---|---|---|
| 1 | 03383000 | Tradewater River at Olney, KY |
| 2 | 04296000 | Lack River at Coventry, VT |
| 3 | 02349900 | Turkey Creek at Byromville, GA |
| 4 | 14185000 | South Santiam River below Cascadia, OR |
| 5 | 05484000 | Raccoon River at Van Meter, IA ST |
| 6 | 06892000 | STRANGER C NR TONGANOXIE, KS |
| 7 | 10255810 | Borrego Palm NR Borrego Springs, CA |

The above catchments and their specific results are discussed in more detail below. In addition to the development of the root storage deficit, average input and output parameters such as effective precipitation, runoff, potential evaporation and transpiration are given. These are determined separately for each year and are indicated by the mean value of the respective year.

### 4.1.1. catchment results:

In most areas, the root storage deficit calculations correspond to an expected range of values in which annual variations occur and reflect a realistic result. As shown in Figure 6, two time series are identified in which the root storage deficit periodically increases in the summer months and records a decrease in the winter. Although the magnitude of the deficit is different due to $E_{pot}$ and latent heat, the values of the two-time series are within realistic values. The temporal offset of the root storage maxima is not obvious at first glance but is explained in more detail below as time lag. For catchment 03383000 this is comparatively small with an average value of 36,5 days for each year. The time lag of the other catchments is listed in Table 2.

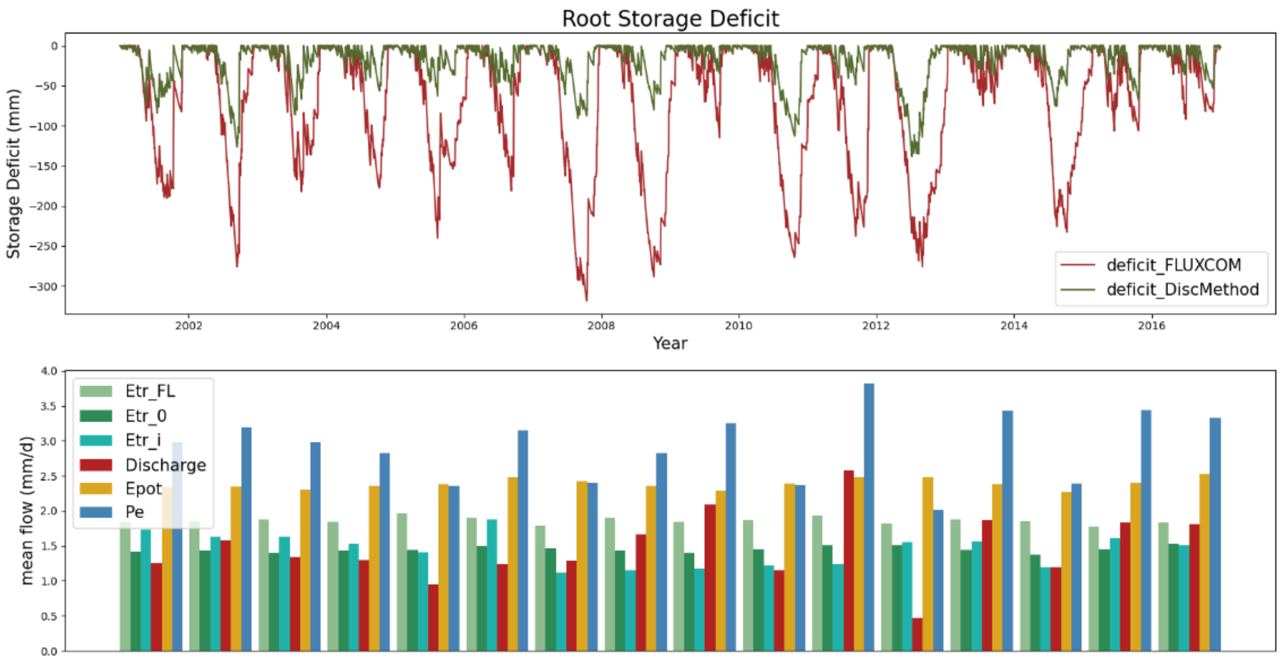


Figure 6: Illustration of root storage deficit (mm) on the Tradewater River at Olney, KY(03383000) derived from the CHIRPS dataset including annual mean values used.

When analysing the catchment areas, it is additionally noticeable that the temporal offset of drought seems to be negligible but the expression of the root storage deficit differs strongly in both methods. In 2002, for example, the difference between the calculated maxima of the root storage deficit is about 150 mm. In 2007, this difference is 200 mm. If the calculated maxima were true, their magnitude would result in significantly different consequences of root formation. Thus, in 2007, the FLUXCOM method shows an increased root zone expansion requirement compared to the Discharge method. The attached input parameters show that the water balance is closed as expected and transpiration occurs. As shown in Figure 6, the average transpiration in the zero iteration in 2001 is about 1.2 mm per day. After optimizing the transpiration coefficients, the average daily transpiration is about 1.8 mm per day. Other parameters, such as the average daily values of potential evaporation $E_{pot}$ (mm/d), effective precipitation $P_e$ (mm/d), and effective runoff (mm/d) in the area, are also within an expected and non-contradictory range. The ratio of $E_{pot}$ to $P_e$ suggests that the Tradewater River near Olney, KY, is an area less at risk of drought compared to other areas. The identified annual variations in maximum deficit can be attributed to the low effective precipitation $P_e$ (mm/d) and the low average annual transpiration values of $E_{tr_{FL}}$(mm/d) and $E_{tr_i}$ (mm/d). The 2004 and 2012 results shown in Figure 7 illustrate this as an example. Note that $E_{tr_0}$ is the transpiration at the first estimate or at the zero iteration. $E_{tr_i}$ is the transpiration after optimization of the transpiration coefficients.

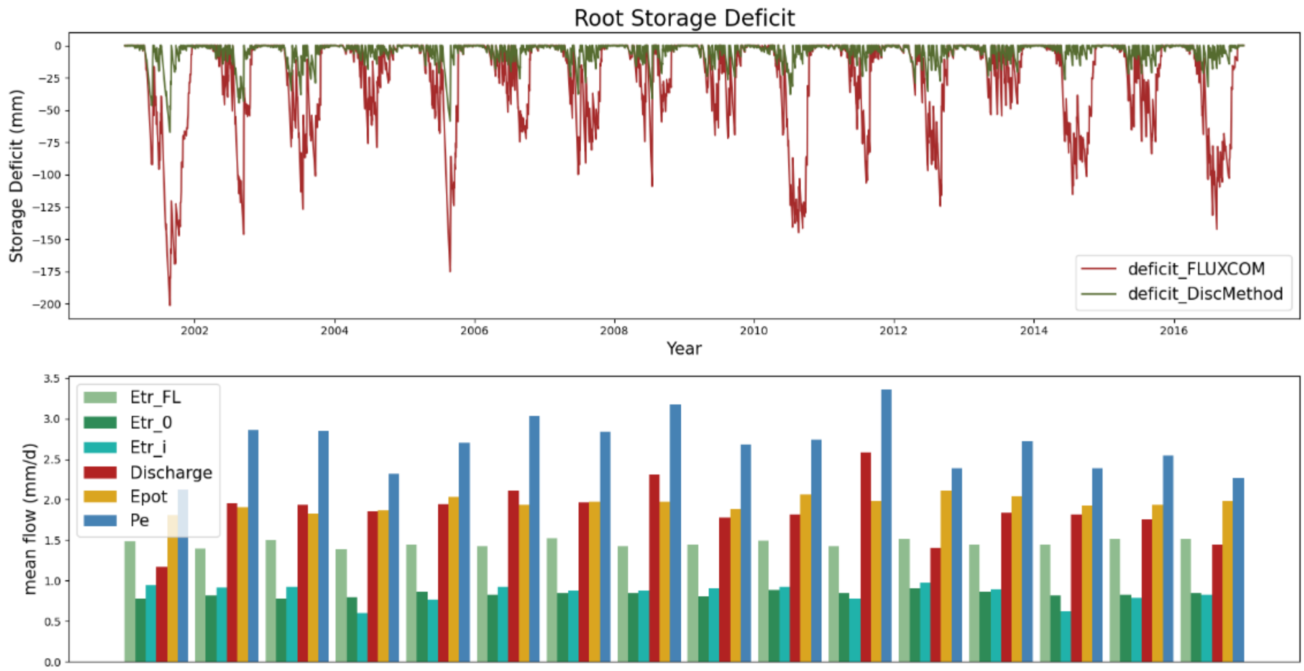


Figure 7: Illustration of root storage deficit (mm) on the Lack River in Coventry, VT (04296000) derived from the CHIRPS dataset including annual mean values used.

There are also small variations in the temporal occurrence of the root storage deficit in catchment 04296000. The absolute differences in the extent of drought are also comparatively small, with a maximum difference of about 150 mm in 2001. However, the relative offset in root storage deficit maxima is uniformly a factor of 3.

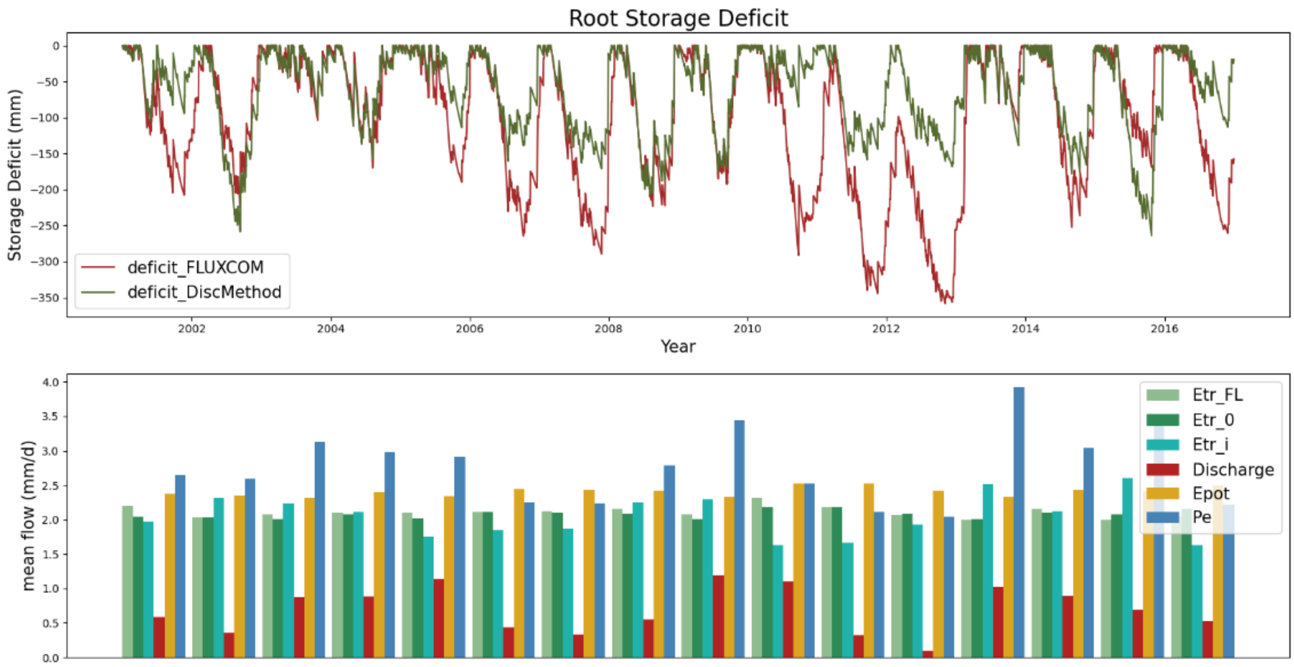


Figure 8: Plot of root storage deficit (mm) at Turkey Creek in Byromville, GA (02349900) derived from the CHIRPS dataset including annual mean values used.

Figure 8 and Figure 9 There are also small variations in the temporal occurrence of the root storage deficit in catchment 04296000. The absolute differences in the extent of drought are also comparatively small, with a maximum difference of about 150 mm in 2001. However, the relative change in root storage deficit maxima is uniform, meaning that the calculated root storage deficits are coherent except for a minor difference in magnitude. The root storage deficit calculated with the FLUXCOM dataset did not fully regenerate from 2011 to 2012. The associated mean values show that this is due to the relatively low effective precipitation in these years compared to the overall average.

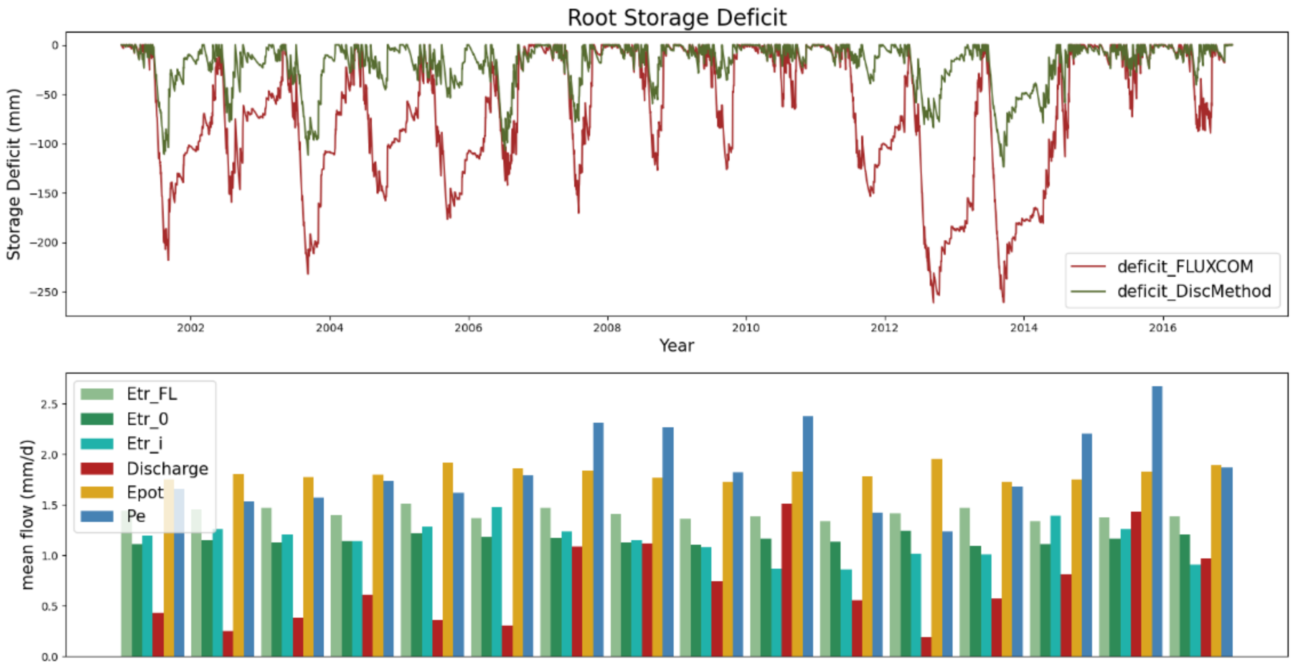


Figure 9: Illustration of root storage deficit (mm) on the Raccoon River at Van Meter, IA ST (05484000) derived from the CHIRPS dataset including annual means used.

Similar to Figure 8, Figure 9 and Figure 10 also show irregularities in periods of lower effective precipitation from 2012 to 2013. Again, it is noticeable that the effective precipitation in the mentioned years is comparatively low.

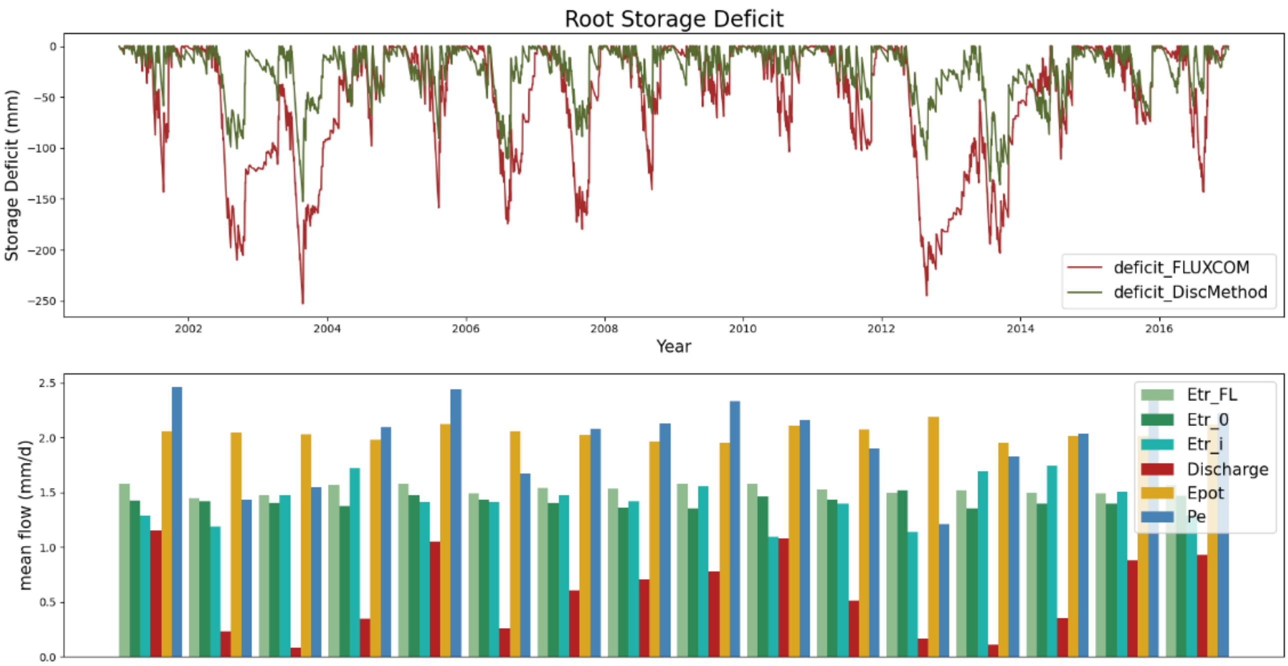


Figure 10: Plot of root storage deficit (mm) in STRANGER C NR TONGANOXIE, KS (06892000) derived from CHIRPS dataset including mean values used annually.

Figure 10 shows, as in Figure 8 and Figure 9, that the respective maxima are generally closer together but in some outliers this difference increases sharply. In addition, there are consecutive years in which the difference in the extent of drought deviates sharply from the general trend. The results for catchments 14185000 and 10255810 lead to contradictory results, which are further explained in the appendix.

### 4.1.2. Distribution of max

To gain a more detailed insight into the relationships between the calculated maxima of root storage capacity, the respective maximum extent of root storage deficit is calculated, as shown in Figure 11. Due to the error shown in Figure 35, catchments where the maximum extent exceeds 1 m are excluded from the analysis as this exceeds the potential root growth capabilities and for this reason is not considered realistic (Ying et al., 2017). Figure 11 shows that the watersheds where the absolute maximum FLUXCOM deficit is found are concentrated in the Midwest.

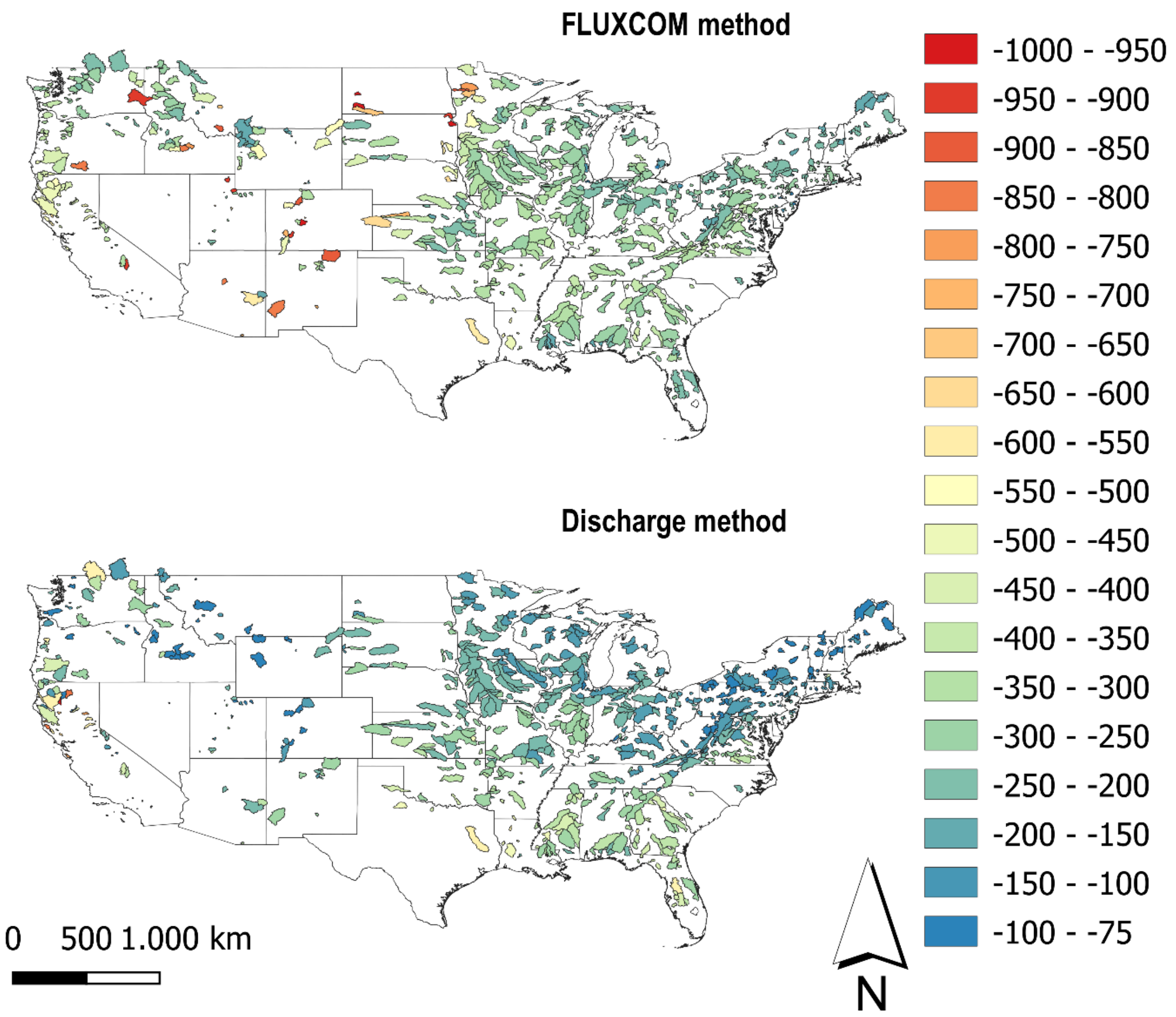


Figure 11: Distribution of maximum storage deficit $S_{tr}d_i(t_0, t_1)$ for the period 2001-2016 (mm) derived by applying the latent heat of FLUXCOM dataset and the runoff method by applying CHIRPS precipitation.

### 4.1.3. Correlations

To determine annual variations in root storage deficit, in addition to the holistic maximum values of the time series from January 1, 2001 to December 31, 2016, annual maxima are also analysed separately. To determine the relationship between the two calculated annual trends in root storage, the correlations of their annual maxima are determined. For this purpose, the corresponding Pearson and Spearman coefficients are calculated for each catchment. Only the maximum annual deflection is correlated and not the time series as such. This is done because the maximum deflection has a higher information content for the extent of potential droughts than the knowledge of what happens the remaining time of the year. The Spearman and Pearson coefficients calculated for each catchment are shown in Figure 12.

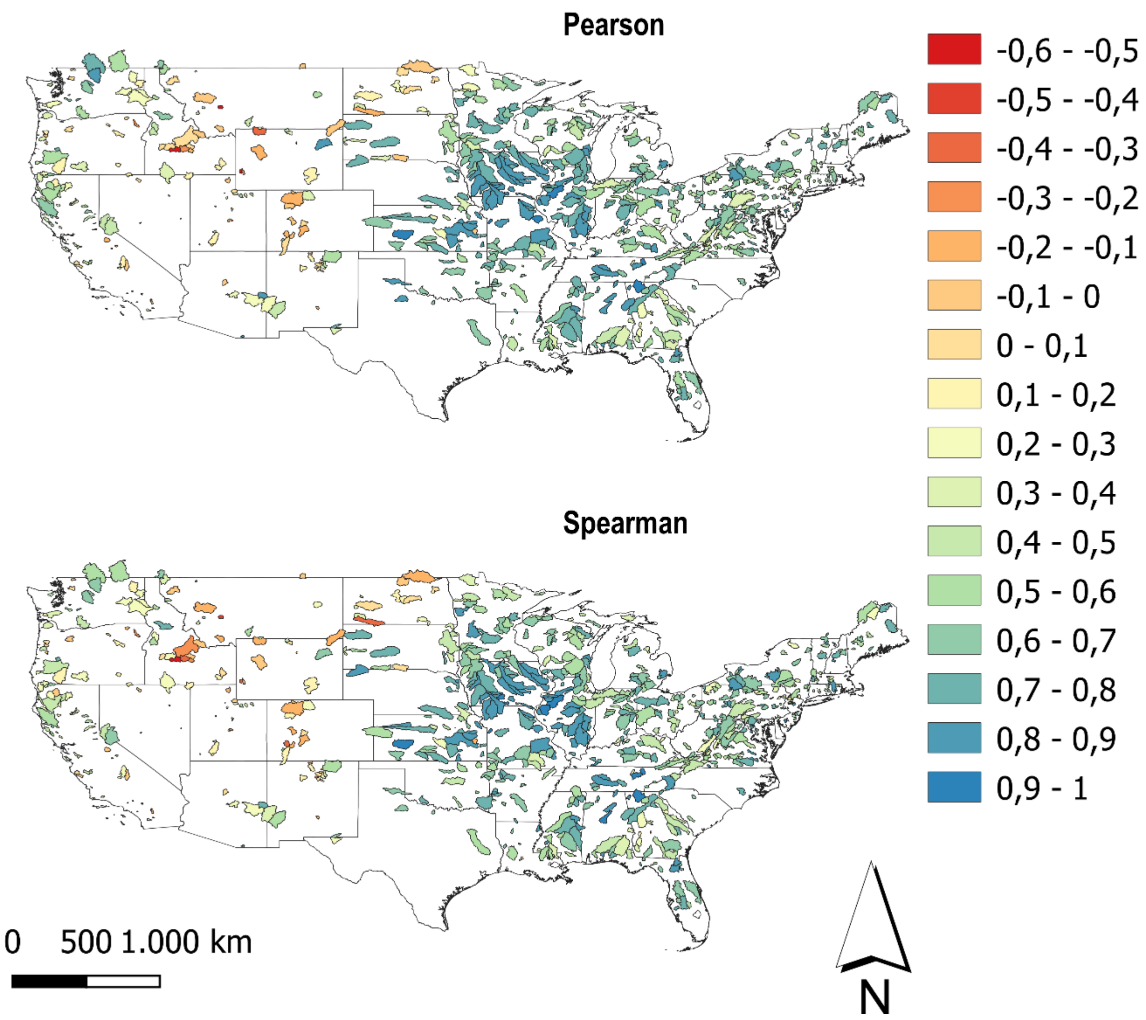


Figure 12: Calculated Pearson and Spearman coefficients (-) for the annual root storage deficit maximum, once using the runoff method and once using the FLUXCOM energy fluxes dataset. Coefficients between 0.4 and 1 are considered sufficiently strong correlation.

As can be seen in both figures, the areas with low correlation are found in the Midwest. Since these results also depend on precipitation supply, it can be assumed that the correlation of root storage deficit maxima depends on precipitation supply. For this purpose, the areas are subdivided according to their average aridity index, as shown in in the Appendix. The aridity index is added as an elementary parameter to each river basin.

## 4.2. Combined Results

In summary, differences in the extent of the root storage maximum are due to variations in effective annual precipitation. To investigate this further, not only the amplitude of the fluctuations but also their timing, also referred to as time lag, was examined. Time lag is defined as the difference between $t_{S_{tr_i.max}}$ (days), the day of maximum root storage deficit of the runoff method, and the day of maximum FLUXCOM root storage deficit $t_{S_{tr_{iFL}.max}}$ (days), as given in equation 16.

$$time\ lag = t_{S_{tr_i.max}} - t_{S_{tr_{FL}.max}} \tag{16}$$

The total bias is defined as the sum of the annual difference between the maximum of the runoff method and the maximum of the FLUXCOM method. The average annual time lag is defined as the sum of the absolute difference in days on which a maximum occurs. The total maximum time lag is defined as the difference in time of the days on which the absolute maxima of the respective root storage deficits occurred over the entire 16-year period. The framework parameters of the respective catchments are shown in the following table for the selected catchments.

Table 2: Summarised CHIRPS results of the selected catchment areas

| Site number | Total bias (mm) | Avg annual time lag (days) | Overall max time lag (days) | Aridity Index (-) |
|---|---|---|---|---|
| **03383000** | -2036,4 | 36,5 | -1727 | 0,658 |
| **04296000** | -1296,2 | 30,4 | 0 | 0,598 |
| **02349900** | -1248,1 | 45,8 | 1084 | 0,719 |
| **14185000** | -4895,0 | 273,6 | -5369 | 0,517 |
| **05484000** | -1493,1 | 14,4 | 369 | 0,733 |
| **06892000** | -1088,5 | 14,2 | 0 | 0,776 |
| **10255810** | -22426,9 | 36,1 | -2917 | 3,764 |

As can be seen in Table 2, what the individual basin analysis suggests is confirmed: In catchment 14185000 and 10255810 the total bias and the maximum total lag are significantly higher than in the other catchments. The high average annual lag of catchment 14185000 can be explained by the fact that no extreme values are available for the runoff method and thus the first January of a year provides the highest value, which drives up the average annual lag.

### 4.2.1. Categorization

In order to establish a relationship between the dryness in the catchments and the correlation of the root storage deficit, the correlations were divided into dryness ranges and presented as a boxplot in Figure 13 and Figure 14. The division was made so that for categories 1 and 2, wet catchments are separated into two classes, and in the remaining categories, 3 through 7, the range of drought indices is fully represented. The maximum added in category 7 is to account for outliers and catchments where the physical maximum was exceeded, as shown in Figure 35.

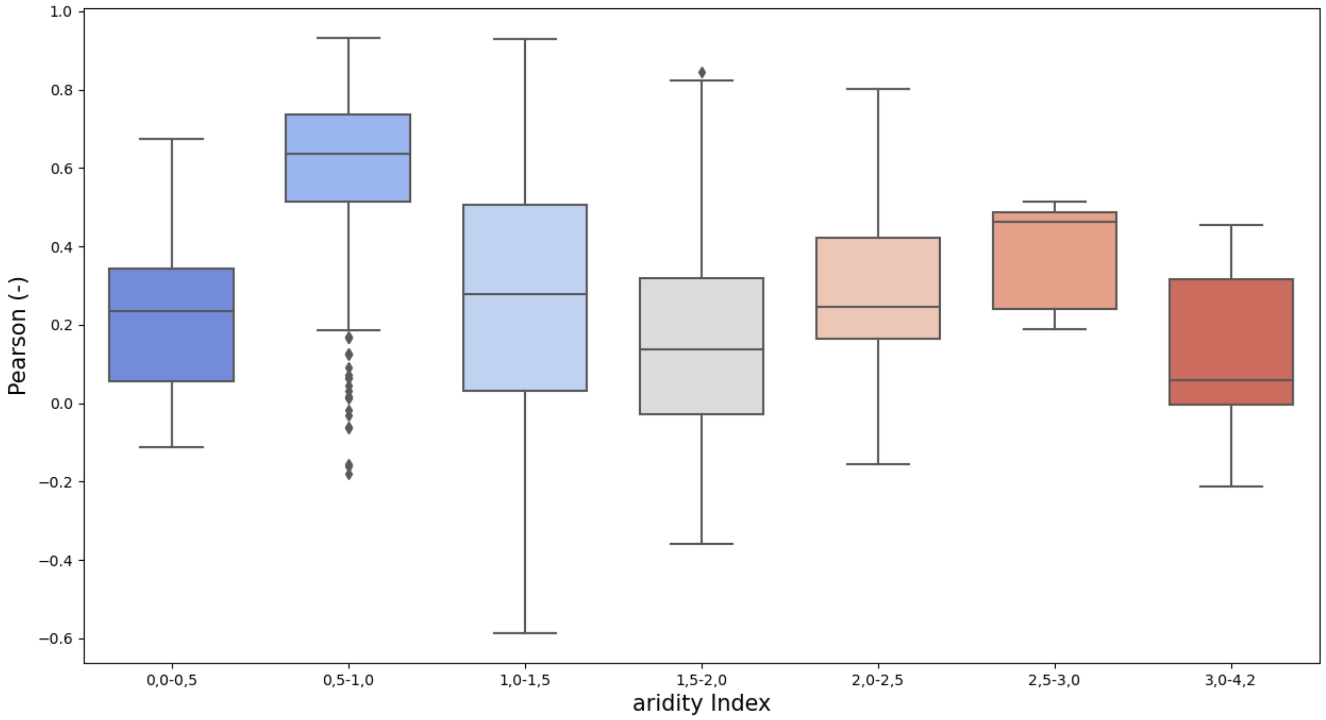


Figure 13: Boxplot of the Spearman correlation per class using the CHIRPS dataset. As can be seen in the figure, both the range and the median of the correlation values for the dryness indices from 0 to 1 are above those of the other aridity indices.

As shown in Figure 13 and Figure 14, drought indices with correlation ranges from 0,4 to 1 have proven to be sufficient. In both boxplots it can be seen that only catchments with drought indices in the range of 0,5 to 1 have sufficient median correlation values. This means that the extent of the respective root storage capacity maxima depends on the precipitation supply and thus primarily on the CHIRPS precipitation dataset. The temporal difference between the absolute maximum of the Discharge method and the FLUXCOM maximum is shown for the CHIRPS dataset in Figure 15 relative to the aridity index.

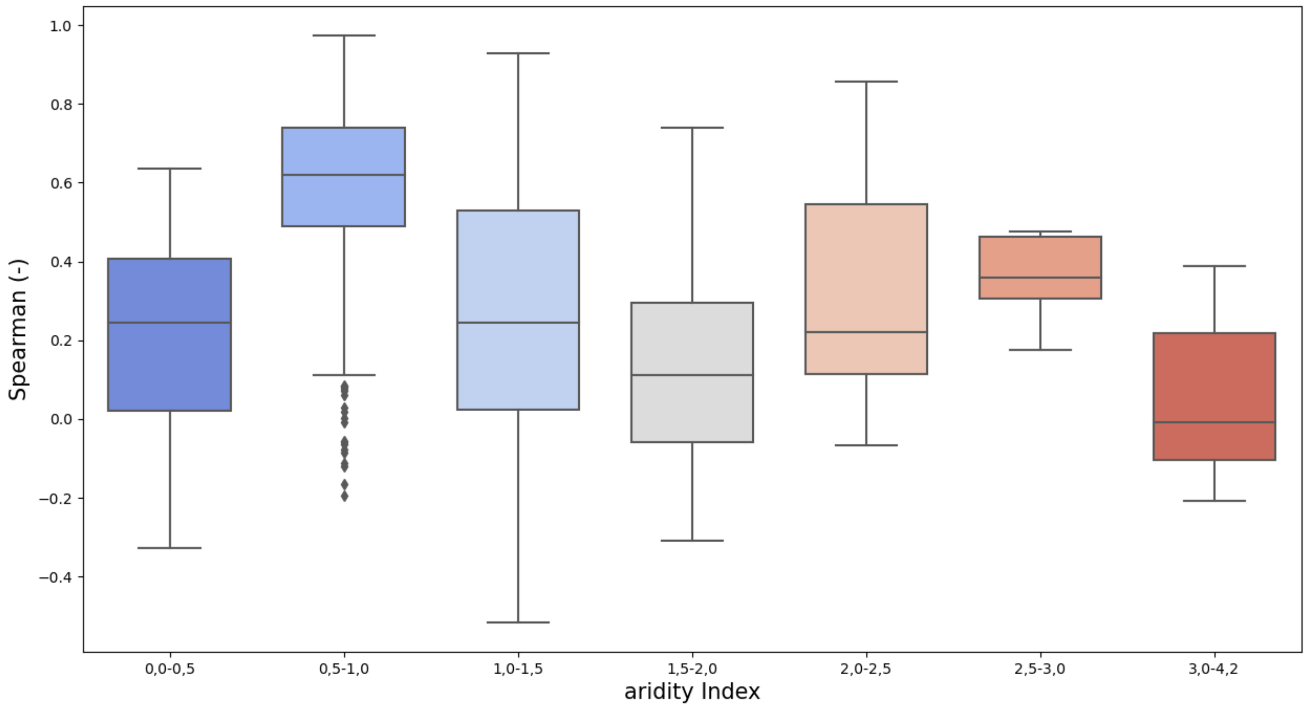


Figure 14: Boxplot of Pearson correlation per class using the CHIRPS dataset. As can be seen in the figure, both the range and the median of the correlation values for dryness indices from 0 to 1 are above those of the other aridity indices.

As shown in Figure 15 and Figure 16, aridity indices with correlation ranges of 0,4 to 1 have proven to be sufficient. In both boxplots it can be seen that only catchments with aridity indices in the range of 0,5 to 1 have sufficing correlation coefficients. This means that the extensions of the respective root storage capacity maxima depend on the precipitation supply and thus primarily on the CHIRPS precipitation dataset. The temporal difference between the absolute Discharge method maximum and FLUXCOM maximum relative to the aridity index is shown for the CHIRPS data set in Figure 30.

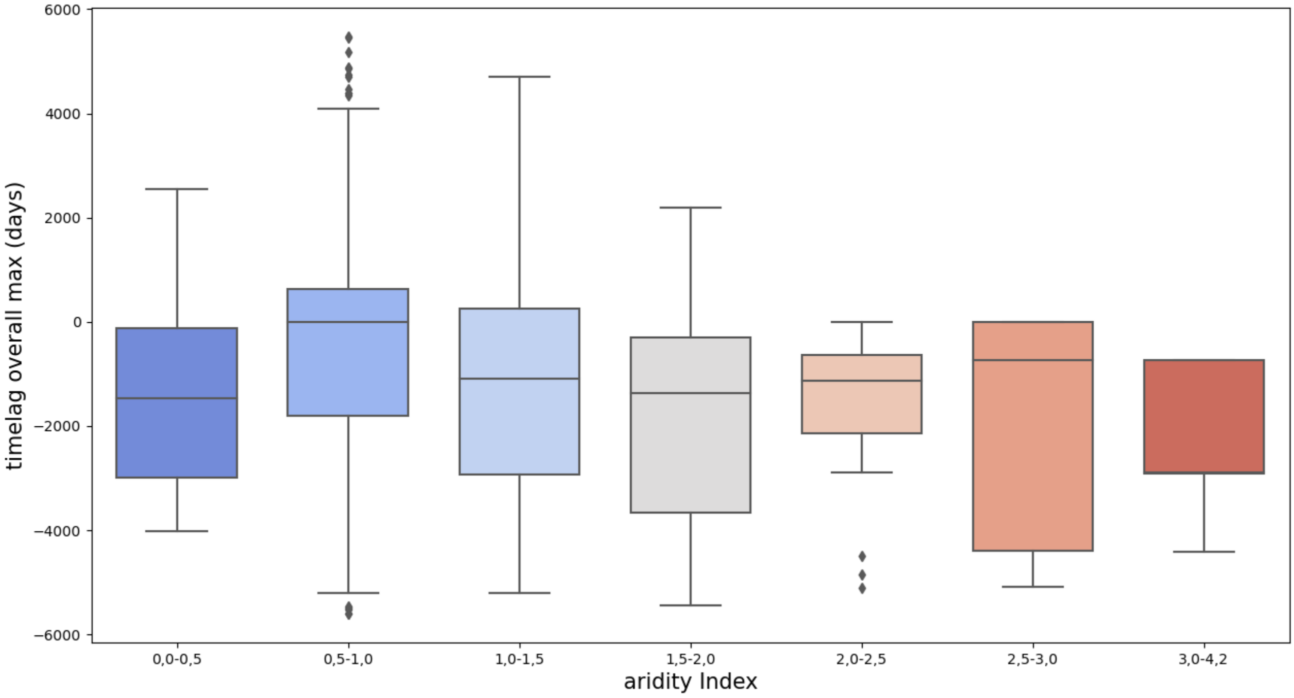


Figure 15: Overall maximum time lag for the Discharge method and FLUXCOM method relative to the aridity index

As shown in Figure 15, the time lag of the fulltime maximum tends to be negative and thus the maximum in the FLUXCOM method occurs temporally after the Discharge method. Also, the biases shown in Figure 16 illustrate that for aridity indices from 0,5 to 1, the distortion is lowest. This means that in these catchments there is the least inconsistency in the methods and that both results correspond to each other to a large extent.

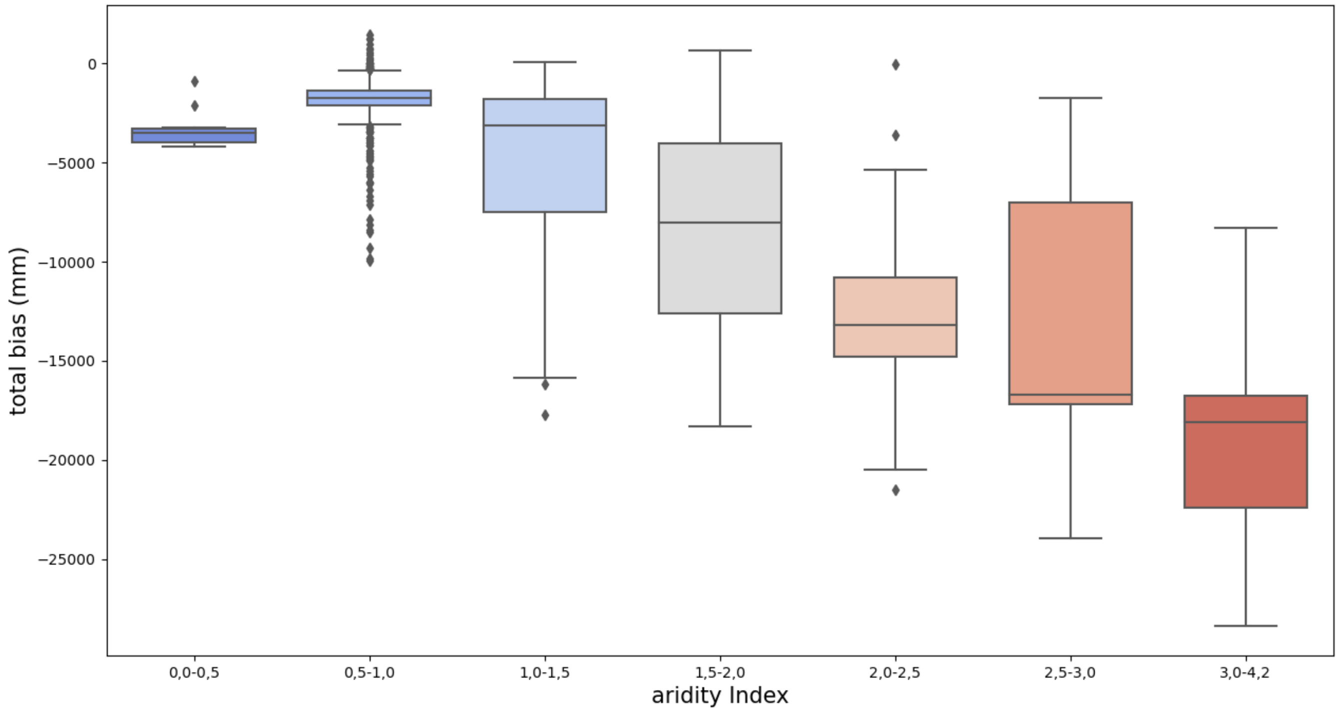


Figure 16: Sum of all annual distortions of the root storage deficit maxima relative to the aridity index.

## 4.3. Verification of the determined results with the help of the CRUNCEP data set.

To illustrate the dependence of the development of the root storage deficit on the effective precipitation, the calculation steps described in 4.1 were repeated with the CRUNCEP data set and thus the CHIRPS results were checked for their validity. This allows identification of possible errors in the determined root storage deficits with respect to the added precipitation data. Indirectly, it also allows justification of the FLUXCOM-RS+METEO product, since the CRUNCEP dataset is the dataset relied upon in the machine learning approach in the RS+METEO product. For accessibility reasons, only version 7 and not version 8 of the CRUNCEP data was used. The individual results for the catchments already investigated in chapter 4.1 are presented below and compared to the results obtained with the CHIRPS data set.

### 4.3.1. CRUNCEP results per catchment

This chapter presents the root storage deficits in all catchments and their input and output parameters calculated using the CRUNCEP dataset. Analogous to the CHIRPS data results, there is a clear offset to the deficit determined using the FLUXCOM dataset. In contrast to the CHIRPS results, the CRUNCEP precipitation is lower overall, resulting in even smaller amplitudes of the root storage deficit in the Discharge method. Comparison of Figure 6 with Figure 17 shows that for the catchment 03383000 also the average $P_e$ is smaller and thus the results of the CRUNCEP data set show a lower value than for the CHIRPS data set. Consequently, the CRUNCEP root storage deficits are also smaller than the CHIRPS root storage deficits.

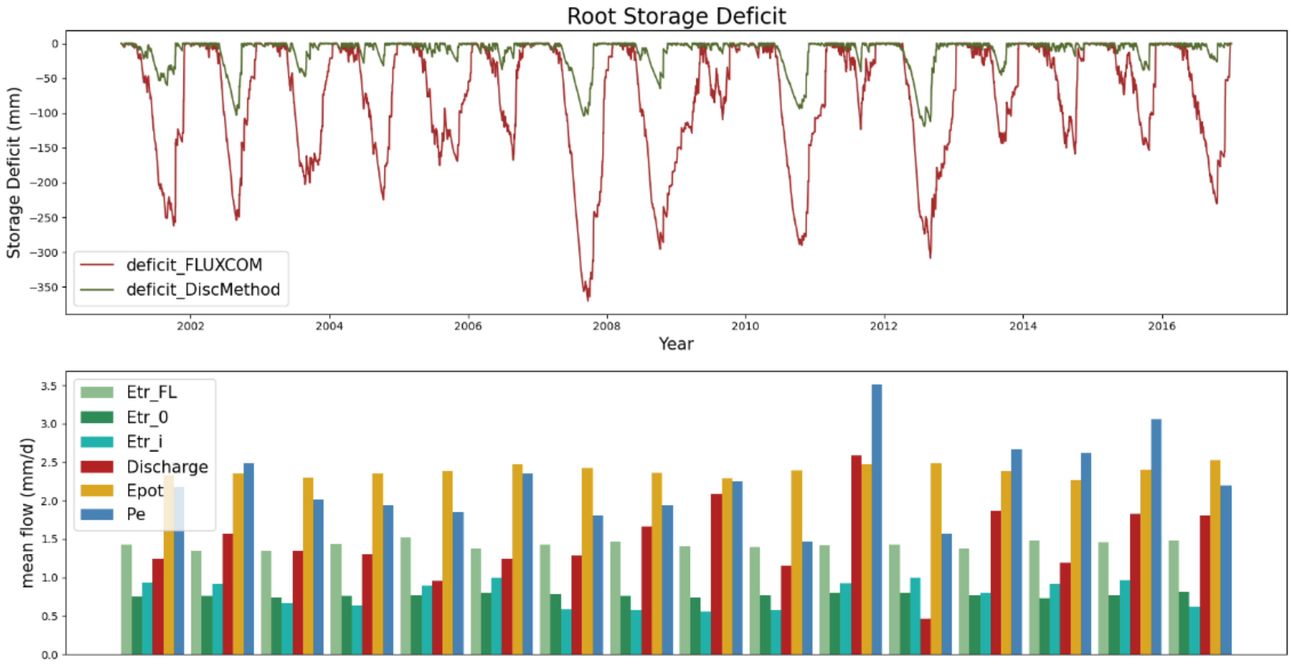


Figure 17: Plot of root storage deficit (mm) on the Tradewater River at Olney, KY IA ST (03383000) derived using the CRUNCEP dataset, including visualization of calculated annual mean values (mm/day).

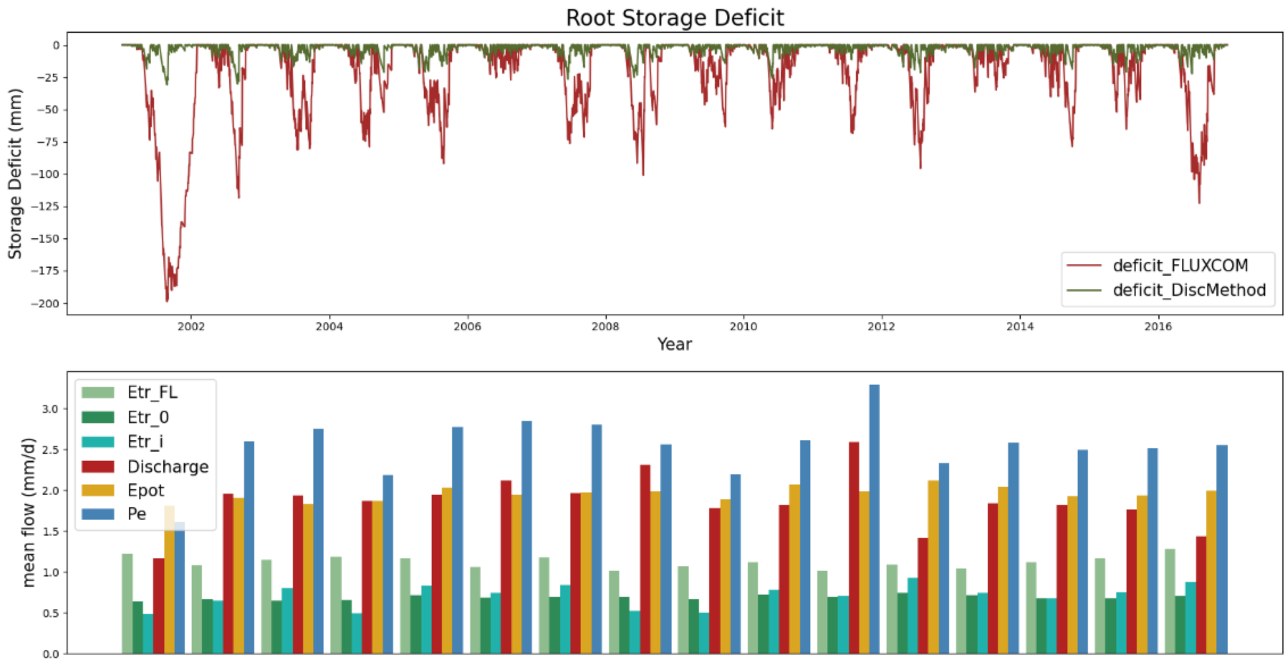


Figure 18: Illustration of root storage deficit (mm) on the Lack River in Coventry, VT(04296000) derived from the CRUNCEP dataset, including visualization of calculated annual mean values (mm/day).

Figure 18 shows that the bias of the Discharge method and the FLUXCOM method is comparatively small. Only in the first year, 2000, a disproportionate bias of 150 mm can be seen in the maximum values determined for this year. In Figure 19 and Figure 20 , root storage deficits are highest in 2011 and 2012, as was the case with the CHIRPS dataset. In Figure 21, this occurs in 2013 and 2014. Thus, it can be said that the CRUNCEP dataset does not produce fundamentally contradictory results. However, it is still confirmed that the results of the CRUNCEP dataset are lower than those of the CHIRPS dataset and thus the CRUNCEP dataset suggests lower actual precipitation. This means that the magnitudes of the root storage deficit for the Discharge method for the CRUNCEP results are still lower than those calculated with the CHIRPS dataset.

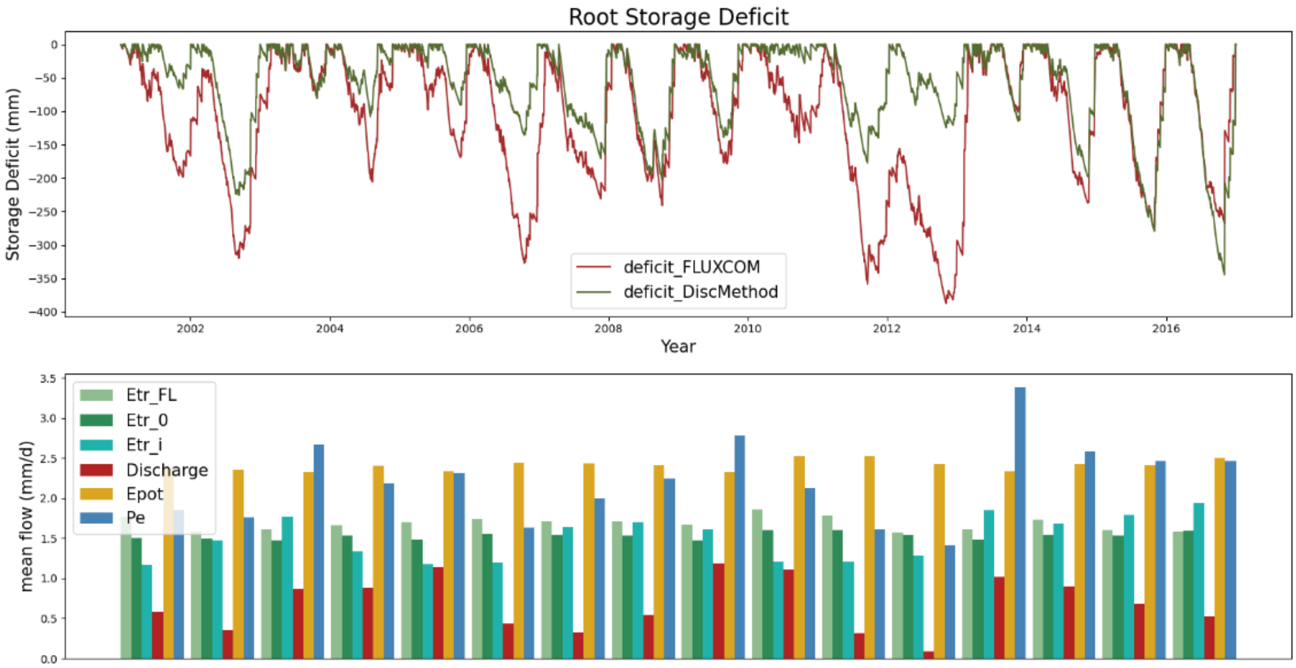


Figure 19: Illustration of root storage deficit (mm) Turkey Creek at Byromville, GA (02349900) derived using the CRUNCEP dataset, including visualization of annual calculated mean forcing in (mm/day).

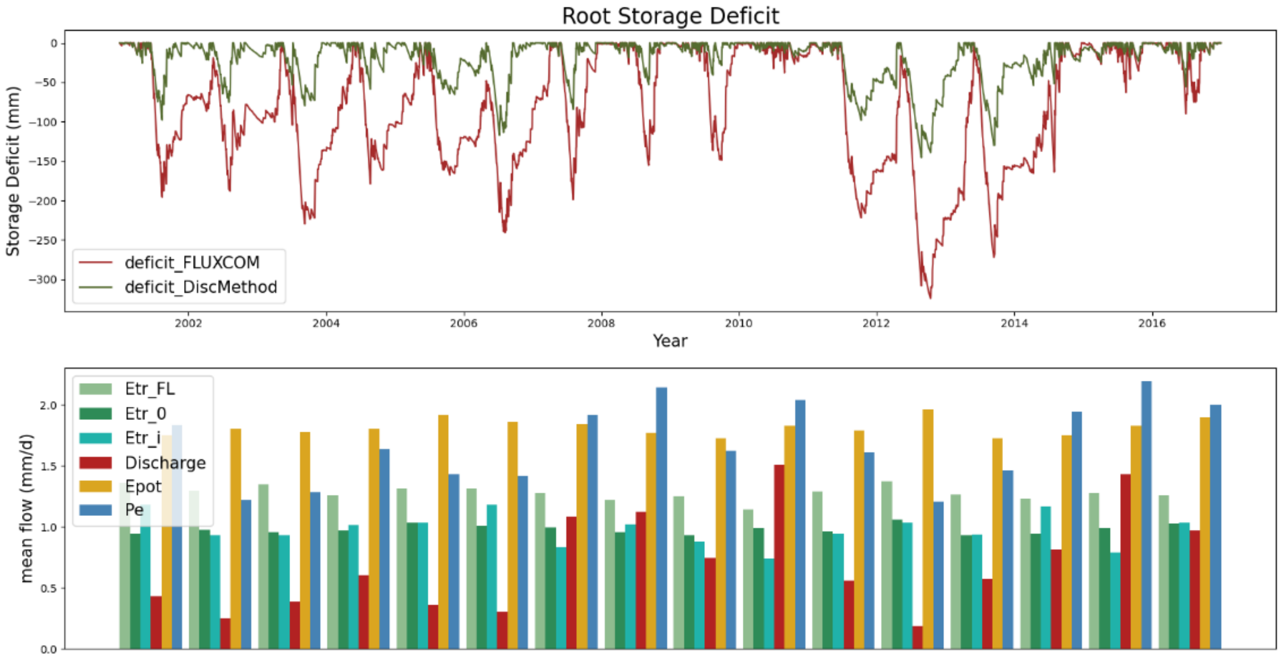


Figure 20: Illustration of root storage deficit (mm/d) on the Racoon River at Van Meter, IA ST (05484000) derived from the CRUNCEP dataset, including visualisation of annual calculated mean forcings in (mm/day).

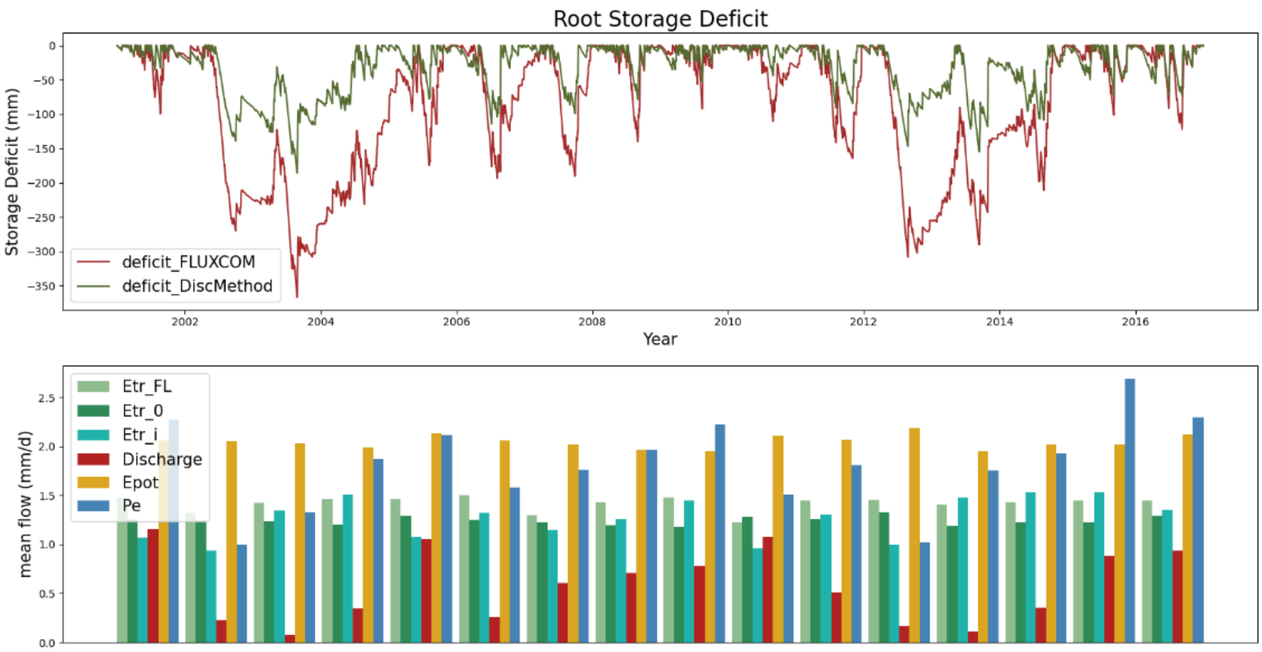


Figure 21: Illustration of root storage deficit (mm/d) Stranger C NR TONGANOXIE, KS (06892000) derived from CRUNCEP dataset.

### 4.3.2. Combined CRUNCEP results

In this chapter, as already determined for the CHIRPS data, the calculated root storage deficits, their maxima and their correlations are presented. Regarding the maximum values of the root storage deficit, it can be said that, as already calculated for the CHIRPS data, only the FLUXCOM method gives deficits of more than 1 meter. These results were also excluded in this work step because it can be assumed that with normal plant growth, these root storage deficits cannot be compensated with increased root growth (Ying et al., 2017). In contrast, the maxima calculated with the Discharge method at a maximum root storage deficit of about 250 mm are in much more realistic value ranges than the maxima of the FLUXCOM root storage deficits shown in Figure 22.

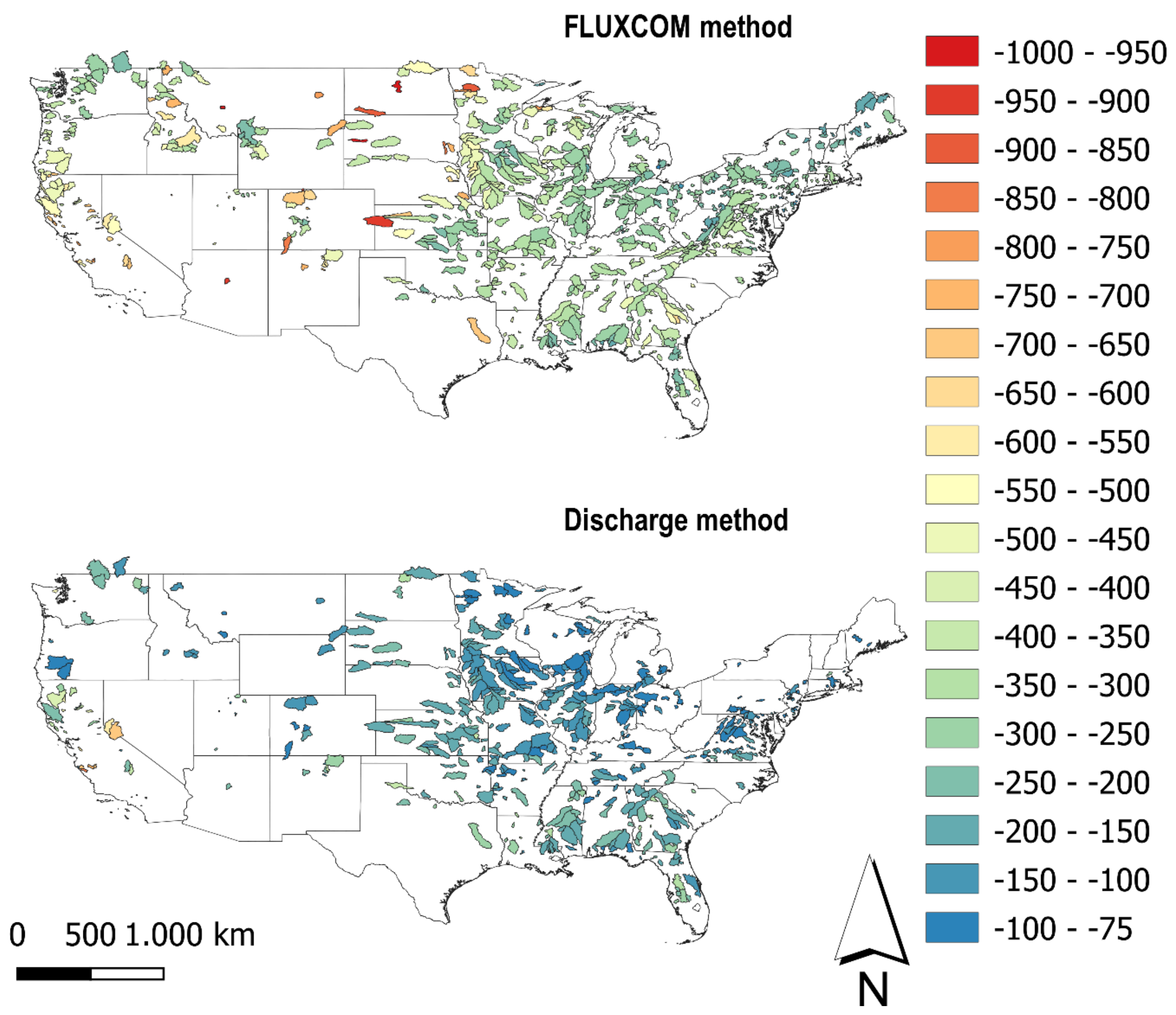


Figure 22: Distribution of maximum storage deficit $S_{tr}d_i(t)$ for the Period 2001-2016 (mm) derived by applying the latent heat of the FLUXCOM dataset and the Discharge Method by applying CRUNCEP precipitation.

For the root storage deficit maxima shown in Figure 22, a comparable spatial distribution as already determined for the CHIRPS data set can be observed. Basically, the catchments with increased root storage deficit are found in the Midwest and not in the East. This again suggests a correlation of the calculated annual biases in root storage deficit to the aridity index. Calculations of Spearman and Pearson correlation coefficients as shown in Figure 23 indicate that negative correlations were determined in the central United States, as was evident with the CHIRPS data set. As with the CHIRPS data, this suggests that the respective root storage deficit maxima are particularly dependent on precipitation supply. To this end, aridity indices were again calculated as listed in the Appendix.

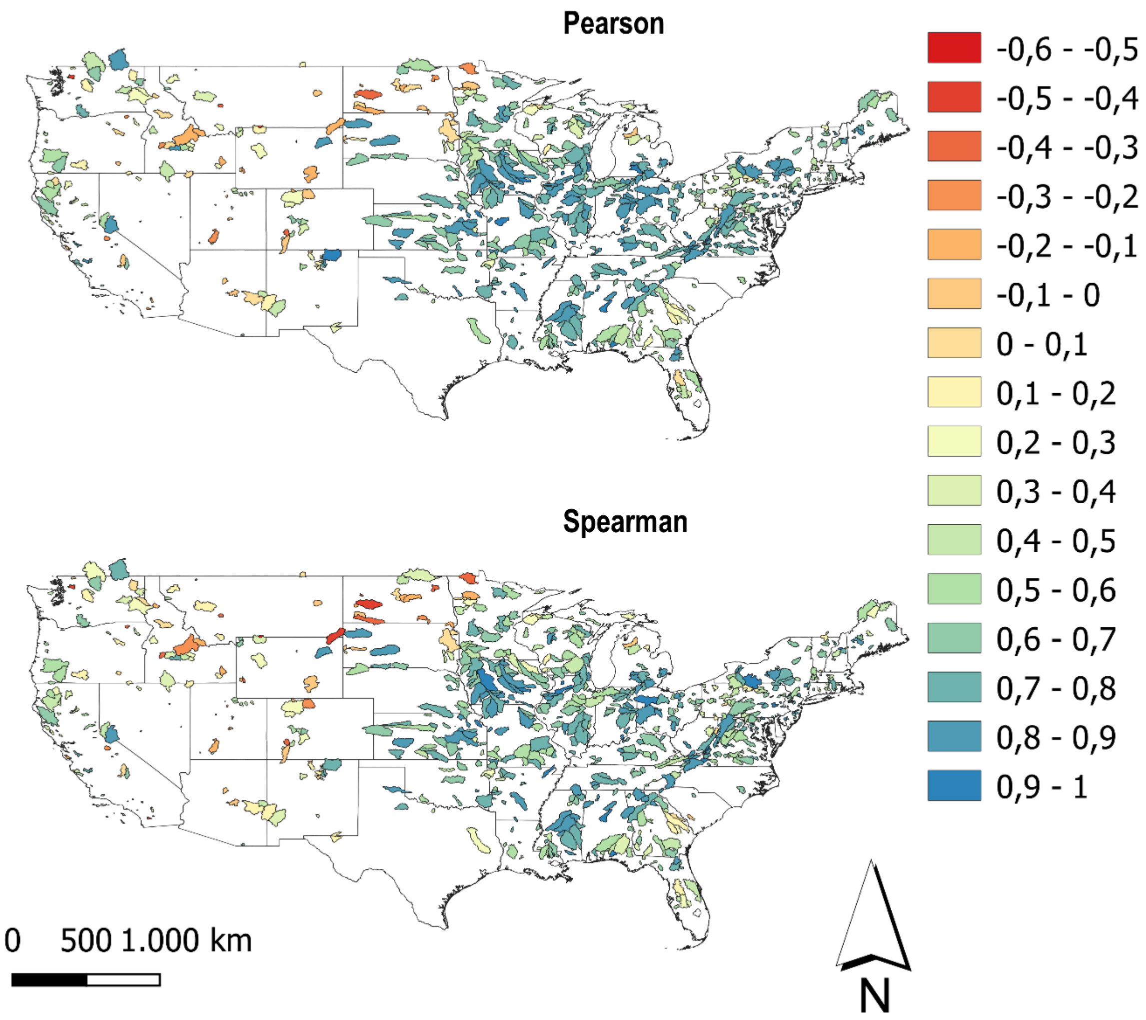


Figure 23: Calculated Pearson and Spearman coefficients (-) for annual root storage deficit maxima, once using the Discharge method (CRUNCEP) and once using the FLUXCOM latent heat dataset. Coefficients between 0.4 and 1 are considered sufficiently strong correlation.

The calculations of the Spearman and Pearson correlation coefficients show that negative correlations occur in the central USA, as was already the case with the CHIRPS data set. As with the CHIRPS data, this suggests that the respective root storage maxima are particularly dependent on precipitation input. For this purpose, the aridity indices were calculated again, as shown in Figure 31.

As with the results obtained using the CHIRPS dataset, the CRUNCEP data again show a high correlation of the annual root storage deficit maxima with the aridity of the catchment, which further emphasizes the dependence on the precipitation dataset. As shown in Figure 24 and Figure 25, the correlation values of the catchments with aridity index 0,5 to 1 are significantly higher than for all other aridity indices.

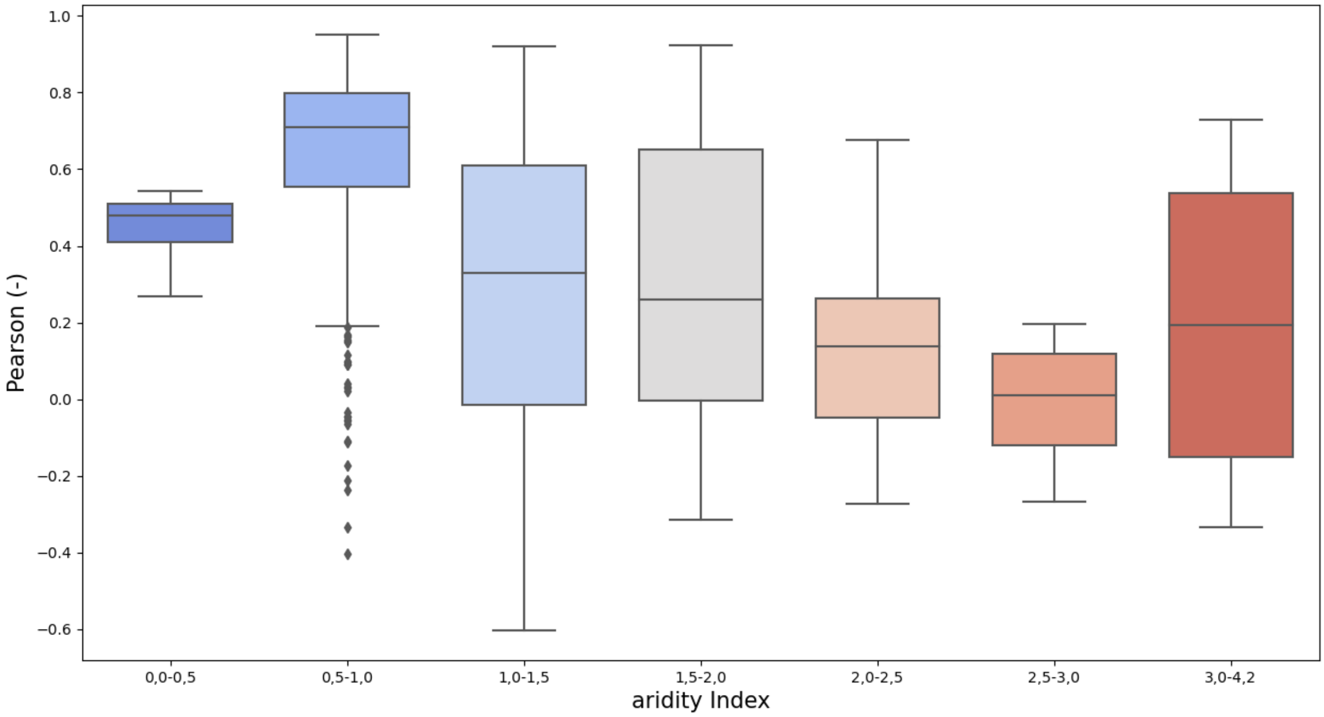


Figure 24: Boxplot of Pearson correlation per class using the CRUNCEP dataset. As can be seen in the figure, both the range and the median of the correlation values for the aridity indices from 0 to 1 are above those of the other aridity indices.

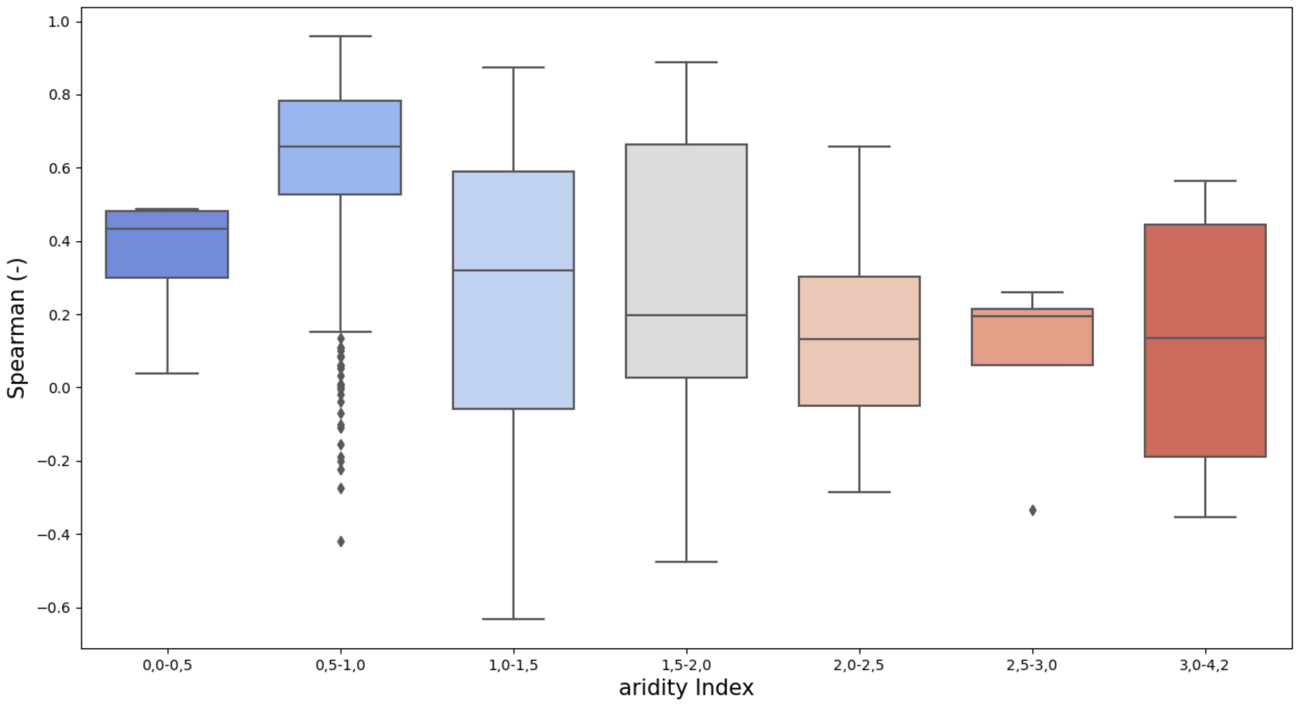


Figure 25: Boxplot of Spearman correlation per class using the CRUNCEP dataset. As can be seen in the figure, both the range and the median of the correlation values for the dryness indices from 0 to 1 are above those of the other aridity indices.

To illustrate the relationship between wet catchments and root storage deficits, the temporal shift of the absolute maxima and the absolute annual bias are shown in Figure 26 and Figure 27. For Figure 26, note that for a value of 0, the congruence in the temporal occurrence of the two calculated root storage deficits is particularly high. As already determined with the CHRIPS data, also for the CRUNCEP results the time lag is particularly low for catchments with aridity index 0-1. When analysing the absolute total bias in Figure 27, it is noticeable that, as for the CHIRPS dataset, only the ranges of aridity index from 0,5 to 1 show a sufficiently low bias in root storage capacity for the CRUNCEP dataset. Total bias, average annual time lag, overall maximum time lag and aridity index were again summarized for the results collected using the CRUNCEP dataset for the selected catchments in Table 3. This confirms that for catchments

14185000 and 10255810 the results differ from those of the other catchments. This is particularly evident in the value of the total bias.

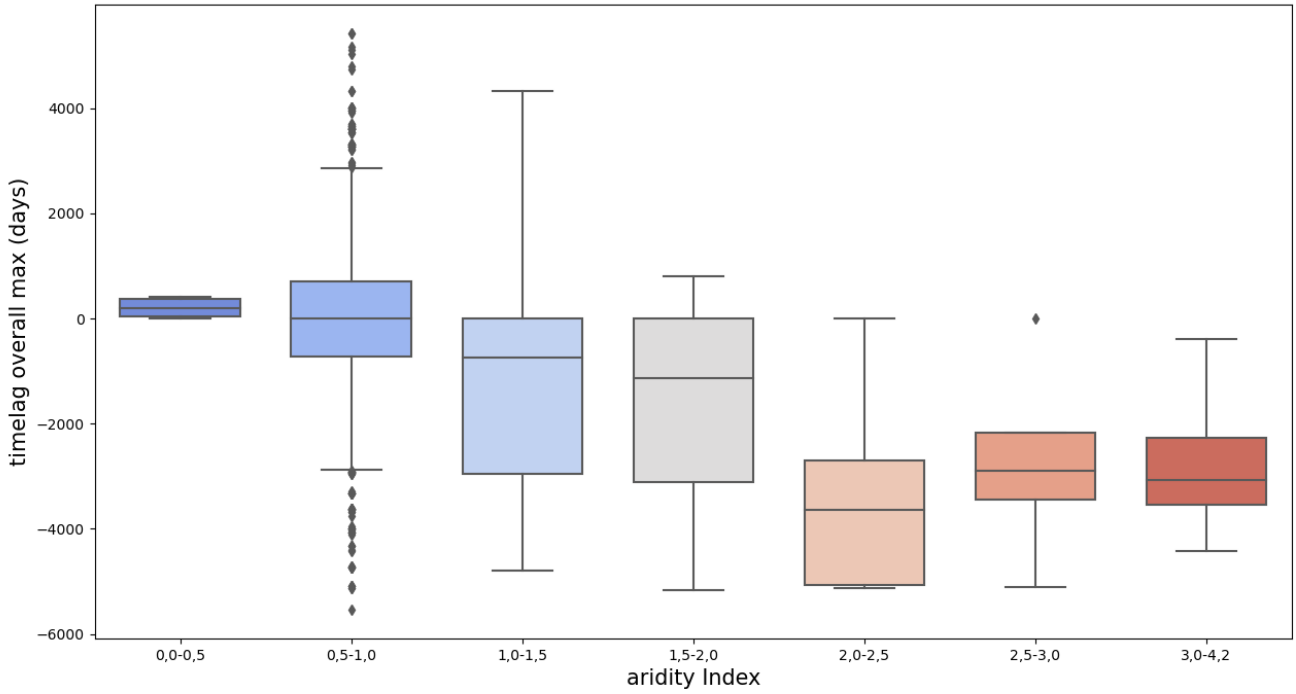


Figure 26: Boxplot of the time lag (days) of the total maxima relative to aridity class.

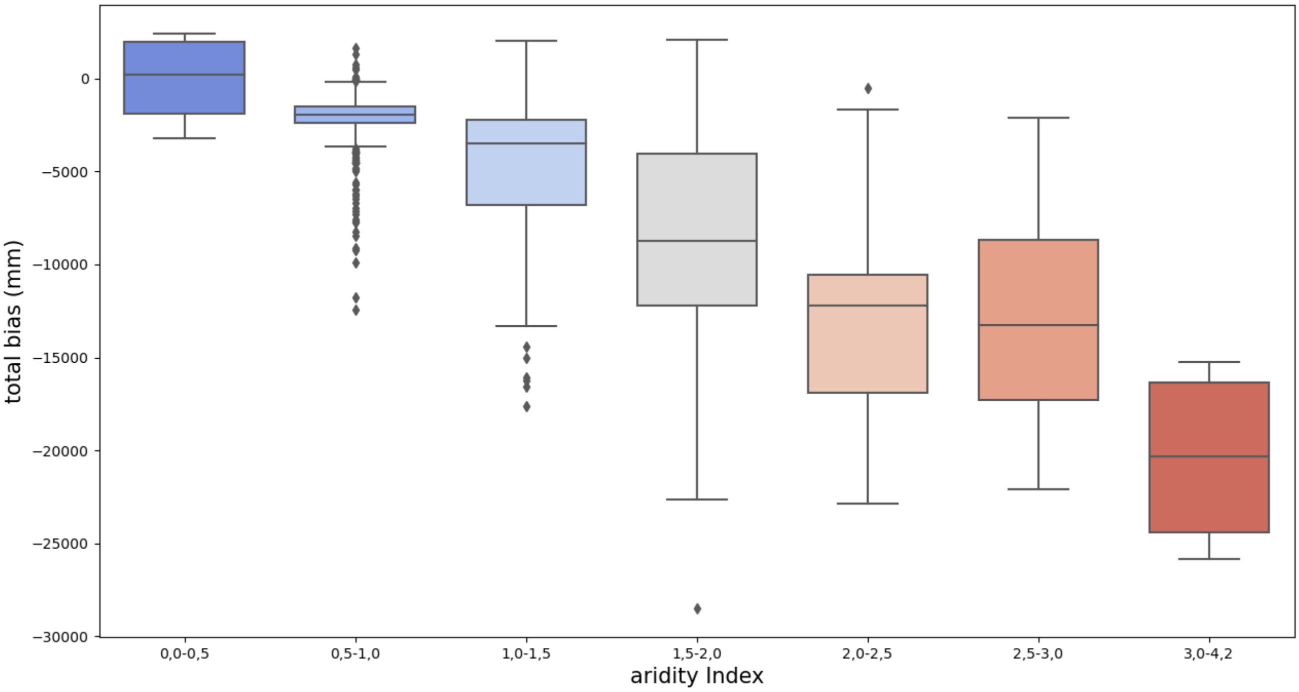


Figure 27: Boxplot of the summed annual distortion (mm) relative to the aridity index.

Table 3: CRUNCEP results of the selected catchment areas summarised.

| Site number | Total bias (mm) | Avg annual time lag (days) | Overall max time lag (days) | Aridity Index (-) |
|---|---|---|---|---|
| **03383000** | -2659,4 | 31,4 | -1772 | 0,699 |
| **04296000** | -1030,7 | 25,9 | 0 | 0,560 |
| **02349900** | -1466,5 | 38,6 | 1458 | 0,745 |
| **14185000** | -5448,4 | 278,5 | -5412 | 0,788 |
| **05484000** | -1680,4 | 32,5 | -49 | 0,743 |
| **06892000** | -1528,2 | 17,7 | 0 | 0,795 |
| **10255810** | -23933,9 | 30,25 | -2888 | 4,247 |

The CRUNCEP data also show that catchments 14185000 and 10255810 have an increased total bias and overall max time lag and the results agree well with those of the CHIRPS data.

## 4.4. Comparison of the results of both precipitation data sets

In summary, the CRUNCEP precipitation dataset confirms the results of the CHIRPS dataset. Since the CRUNCEP precipitation is generally slightly lower than the CHIRPS data set, it is not surprising that the aridity index is higher for the CRUNCEP calculations than for the CHIRPS calculations. With a few exceptions, the overall sum of annual biases for both precipitation data sets also follow the picture shown in Figure 28.

As can be seen there, the total bias is negative in a large part of the catchments. Only in a few catchments is there a positive net bias, shown here in cyan. However, the results with positive total bias are an exception. One of these catchments is located in Florida, in the south of the USA, so that the precipitation values taken as a basis may actually be correspondingly low. A more detailed review is needed here. The identified areas in the north are border areas to Canada, where a direct assignment of the runoff quantity to the catchment area is not possible. In these areas, a fundamentally incorrect result can probably be assumed. The results of the averaged absolute bias are attached.

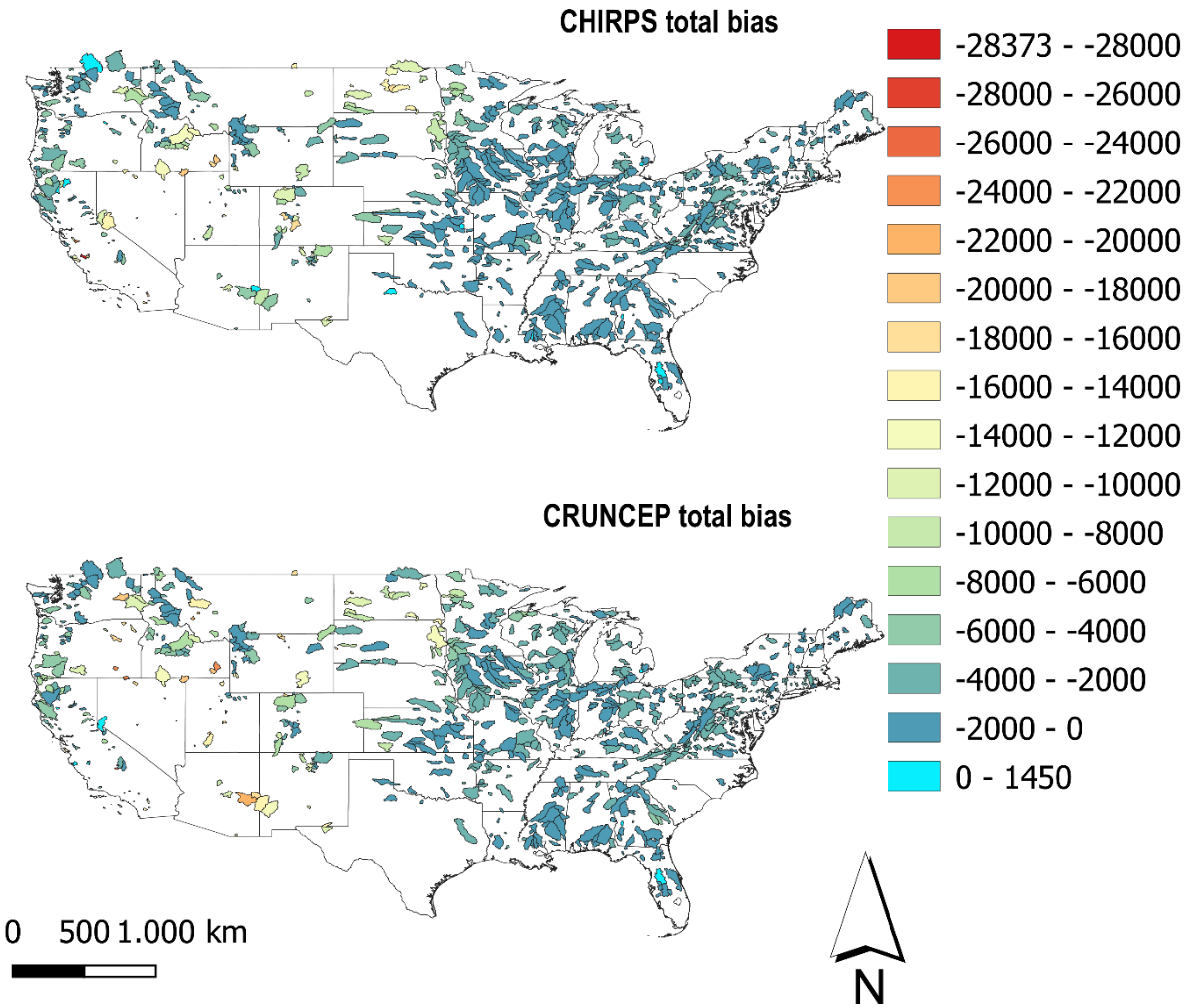


Figure 28: Comparison of total biases (mm) in all catchments for both precipitation datasets.

Catchments in which the previously determined physically justifiable root storage deficit maximum of one meter is exceeded are summarized in Figure 29. It is noticeable that the catchments in which this is the case correspond to the areas in which, as shown in the appendix, an increased aridity index was determined. If these results are summarized for these catchments, it can be concluded that they are in the process of dehydration. Average values of the results of both precipitation data sets are listed in the appendix.

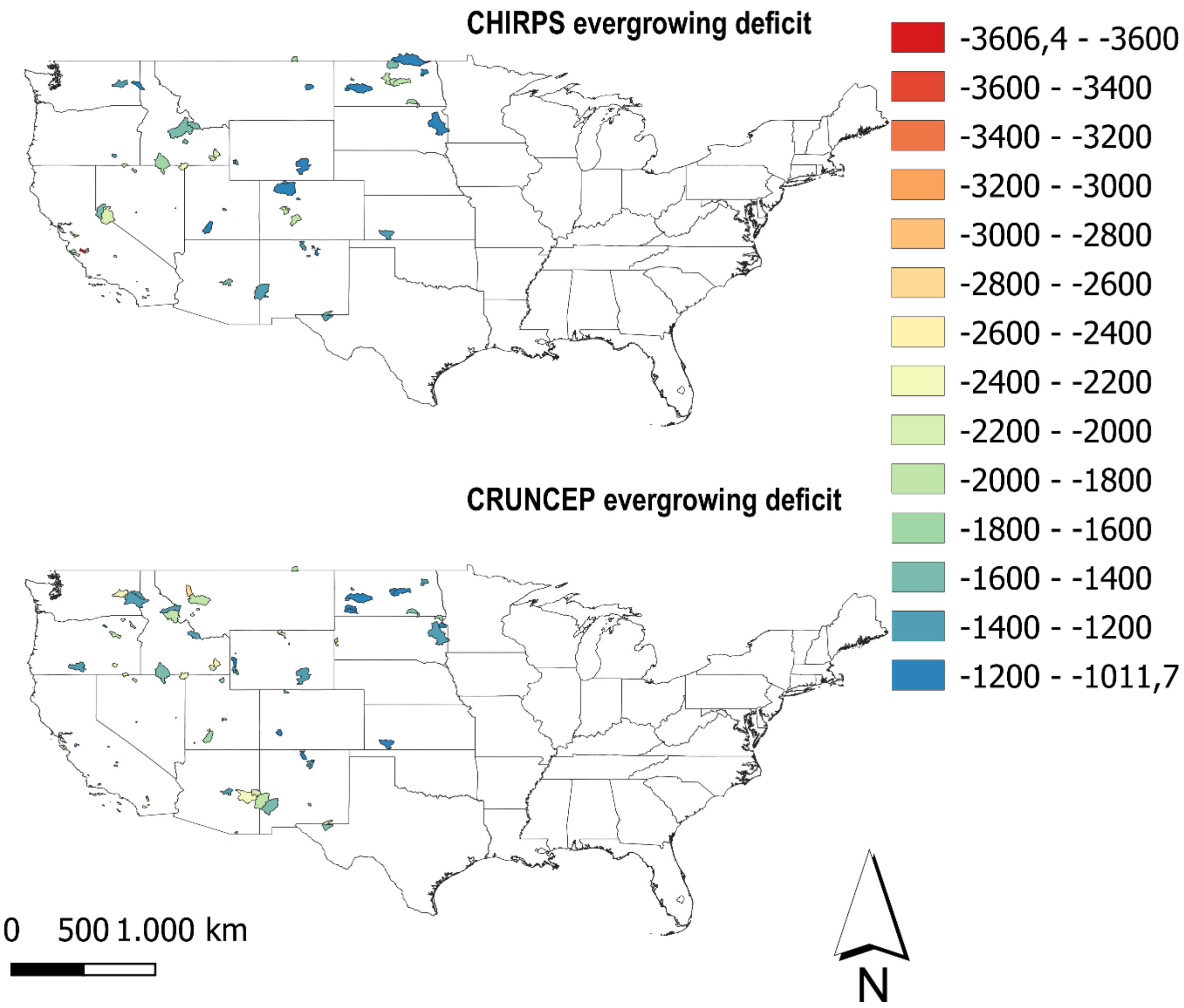


Figure 29: Mapping of the catchment areas in which the root storage deficit grows towards negative infinity.

# 5. Discussion

The calculation of root storage deficits was successfully carried out in 1125 catchments. It can be observed that in a large part of the considered areas a deficit occurs in the summer of one year, which in most cases is replenished in the following winter. In a few cases, the deficits drag on for more than a year, and the recovery does not occur until the following year.

### Ever growing deficit

In a few watersheds, root storage deficits are trending to become "ever growing deficits," so that the transpiration storage for that watershed experiences a steady drying out. This means that in these areas the root storage deficit is steadily increasing, increasing desiccation can be assumed. An appropriate example is watershed 10255810 which is located in Borrego Palm NR Borrego Springs, California, where desiccation of soils appears to be possible in principle based on local conditions.

### No transpiration

The watersheds shown in Figure 34 and Figure 36 where the calculated results appear to indicate no transpiration are those where the Discharge Method framework could not be met. Thus, for catchments where the effective precipitation was calculated to be less than the local runoff and corresponding to equation 3, no transpiration would be possible. The few areas where this was not possible was in arid climates. An example of this is catchment 14185000 on the South Santiam River below Cascadia in Oregon. Since in practice even the smallest amounts of transpiration occur in the driest regions, the missing transpiration determined there is not realistic. To prove the actual facts, it will be necessary to conduct supplemental, possibly empirical, studies (Mitra, 2018).

### All other catchments

In most areas, however, this transpiration could be calculated. For the areas where transpiration was calculated, the following can be summarized:

The FLUXCOM RS+METEO CRUNCEP dataset confirms the droughts calculated with the runoff method. In none of the catchments do the two root storage deficits lead to completely opposite conclusions regarding the temporal occurrence of drought.

In contrast, in catchments where the general conditions for the calculations are not met, a clear temporal offset of the root storage deficit maxima is observed. The temporal offset for the respective methods and selected catchments can be seen in more detail in Table 2, Table 3 and in Figure 32 and Figure 33.

On the other hand, the extents of drought calculated by both methods differ in all areas. Thereby, the deficits calculated by the FLUXCOM method are higher in almost all catchments than the values calculated by the Discharge method (cf. Figure 11 and Figure 22). This general bias assumes variations of up to 500mm in some areas, which does not allow for any serious conclusions to be made regarding the actual root storage deficit. Since in some years this basic bias assumes larger proportions than in others it can be suspected that in these years the basic bias presented is joined by additional effects that increase the existing bias (De Boer-Euser,2019).

As a result, the Discharge method and the FLUXCOM method give more or less divergent results with respect to the extent of the identified drought. Thus, it can be said that the results obtained with the FLUXCOM RS+METEO product suggest greater and later desiccation.

This apparent increased extent of drought can have serious consequences regarding the viability of local habitats. As mentioned in Steudle (2000) and confirmed in Wang-Erlandsson (2020) and van Oorschot (2021), it is explained that the relationship between drought and root storage deficit has not been sufficiently scientifically investigated to make concrete conclusions regarding site unsuitability for local flora. This insufficiently scientifically studied circumstance cannot be resolved in this work.

The agreements of the method-specific results determined in the present work increase with the increasing availability of water in the areas in question. Conversely, this means that with lower water availability, a reduced significance of the determined root storage deficits can be assumed, since the respective results deviate more strongly from each other. However, the suggested deficits may be smaller in practice because external water flows, such as irrigation and groundwater flows, were not considered in the calculations (Vera, 2015).

### Overall maximum

The analysis of the results of the bias of the overall root storage deficit maxima shows that in the catchments where the aridity index is greater than 1, negative correlations of extracted maxima were more severe than in humid river catchments. This shows that the correlations of root storage deficit maxima are higher in humid catchments than in arid ones. When compared with the CRUNCEP precipitation dataset, this dependence on water supply is further reinforced. Thus, differences in the coherence of root storage deficit maxima for changing aridity conditions are present. As can be seen in Table 4 the average bias is not greater than 212 mm in all areas.

### Interpretation

Considering that the FLUXCOM project used MODIS land cover data as the predictor variable, it can be seen that the three machine learning methods used result in the latent heat effectively suggesting higher transpiration values compared to the iteratively calculated transpiration. This is particularly due to the fact that the machine learning was fed with land use data, which allows the respective albedo effect of land use to be included in the consideration. Thus, a higher evaporation can be assumed for sealed areas than for unsealed ones, which could explain the determined deviations.

According to Steudle (2000), root storage deficits are accompanied by pronounced suberization, which negatively affects water transport within the plant. This leads to corking, which permanently reduces the possibilities of water uptake but also evaporation. This affects the water balance by further reducing the ability of the roots to absorb water (Steudle, 2000). Thus, potential desiccation tendencies cannot be clearly quantified as they are consistently increasing in the sense of a positive feedback loop. It can be assumed that in areas, with an increased maximum bias, the pressure on the plants is increased in such a way that it can be assumed that they are in a process of increasing adaptation to a changing site. The effective added value of the Discharge method is thus limited to statements concerning temporary developments within the period under consideration. Continuous existing developments that were initiated before the start of the period under consideration, or that extend beyond it, have given a result that cannot be placed in any relation and does not represent any added value compared to a holistic balancing of the parameters.

The comparative calculation approach using the FLUXCOM latent heat data did not confirm the root storage deficit maxima and their temporal occurrence. The insight into the root storage deficit calculation is lacking concrete field measurements on which they could be linked. It was confirmed that the results of the Discharge method can be used as an indicator of desiccation as long as this development starts and is completed within the period under consideration. This means that deficits in the water balance of plants can only be assigned if this root storage deficit can be compensated within the observation period. In contrast to these, more conceptual results, insights into the probable risk of impending desiccation can also be derived. Thus, time lag can be used to infer time periods subject to water stress (Porporato, 2001).

Further insight can be gained by calculating the annual bias. For example, the correlation of the root storage deficit maxima calculated annually using the FLUXCOM method, as well as the Discharge method, gives a clear overlap with the determined aridity index (compare Figure 30 and Figure 31). In contrast, the holistically calculated root storage deficit maxima (compare Figure 11 and Figure 22) show a large offset between the two methods, which makes concrete conclusions difficult. Therefore, this work does not provide an answer to the question which root storage deficit is to be associated with which concrete consequences for plants and ecosystems.

Thus, the Discharge method offers the opportunity to improve this understanding, as annual maxima of root storage deficit are considered relative to each other and thus specific annual values can be assigned to concrete framework parameters. Supplementary empirical studies are required here if needed. This means that the calculated root storage deficit maxima have to be coupled to concrete values of local devastation in order to assess whether one of the methods reflects reality.

Another added value of the present work results from the transfer of in situ measurements, the local runoff data, into area-wide raster data. This is of particular interest to climate scientists who rely on area-wide information. Thus, the application of in situ measurements can be seen as an enrichment of the cross-consistency test mentioned in the FLUXCOM article. The correlation values and the associated coherence of root storage deficit maxima in humid catchments suggest that for a more accurate determination of actual root storage deficits, their concrete assignment to plant parameters is lacking. Transition Since no specific plant value can be assigned to the root storage capacity threshold. From Steudle (2000), it appears that root zone storage capacity provides information on spatially varying changes in hydrologic characteristics of an area and therefore may be useful to assess changing hydrology under changing conditions. This is tied to the applicability of the water balance-based approach. This assumes sufficiently high local runoff, which does not occur immediately in arid catchments. Thus, the approach used in this work is only recommended in humid catchments. Thus, the calculated root storage deficit maxima say less about the actual extent of drought but only indicate whether it is occurring or not. Within a catchment, the allows us to nevertheless investigate whether intermediate developments of root storage deficits occur, assuming that these re-equilibrate (de Boer-Euser, 2019).

In addition, the values collected can be linked to plant-specific trends to promote optimized, long-term, resilient land use. Future research could assign specific meaning to the magnitude of root storage deficits. For example, critical thresholds for plants could be defined so that root storage deficits can be suggested to the transition of an ecosystem and that future root storage deficits can be contextualized with respect to climate change. Their calculation could be tailored to specific climate scenarios and thus helpful with respect to humid conditions of river basins (Sung, 2017).

# 6. Conclusion

In this paper, root storage deficit calculations were successfully performed in 1125 watersheds in the U.S. for the years 2001 to 2016. In doing so, the results provide both absolute and relative insights into root storage deficit trends in river basins in the United States. However, the calculated root storage deficit maxima cannot be attributed to specific consequences in each area. However, annual differences in root storage deficit provide insight into the relative stress experienced by affected plants at their site. River basins that experience a steadily increasing deficit are described as potentially at risk of drying out. However, no concrete consequences for the catchments can be derived from this. Thus, the applicability of the Discharge Method and the FLUXCOM dataset depend on a match with the concrete consequences in the catchments. Thus, field studies are needed to obtain these concrete measurements.

# REFERENCES

De Boer-Euser, T., McMillan, H.K., Hrachowitz, M., Winsemius, H.C., Savenije, H.H.G.; Influence of soil and climate on root zone storage capacity (Open Access) ; (2016) Water Resourcesn Research, 52 (3), pp. 2009-2024. Cited 48 times. ; http://agupubs.onlinelibrary.wiley.com.tudelft.idm.oclc.org/hub/journal/10.1002/(ISSN)1944-7973/ doi: 10.1002/2015WR018115

De Boer-Euser, T., Meriö, L.-J., and Marttila, H.: Understanding variability in root zone storage capacity in boreal regions, Hydrol. Earth Syst. Sci., 23, 125–138, https://doi.org/10.5194/hess-23-125-2019, 2019.

Brenner, C., Frame, J., Nearing, G. et al. Schätzung der Verdunstung mithilfe von Machine- und Deep Learning-Methoden. Österr Wasser- und Abfallw 73, 295–307 (2021). https://doi-org.tudelft.idm.oclc.org/10.1007/s00506-021-00768-y

Ceres.larc.nasa.gov. 2021. CERES – Clouds and the Earth's Radiant Energy System. [online] Available at: https://ceres.larc.nasa.gov/> [Accessed 03 Nov 2021].

Coenders, 2017 lecture Notes: Hydrological Processes and Measurements, TU Delft

Funk, C., Peterson, P., Landsfeld, M. et al. The climate hazards infrared precipitation with stations—a new environmental record for monitoring extremes. Sci Data 2, 150066 (2015). https://doi.org/10.1038/sdata.2015.66 [Accessed 03 Nov 2021].

Gao, H., Hrachowitz, M., Schymanski, S. J., Fenicia, F., Sriwongsitanon, N., and Savenije, H. H. G.: Climate controls how ecosystems size the root zone storage capacity at catchment scale: Root zone storage capacity in catchments, Geophys. Res. Lett., 41, 7916–7923, https://doi.org/10.1002/2014GL061668, 2014. a, b, c, d

Gao H., Peng et al. “Use of double mass curves in hydrologic benefit evaluations.” Hydrological Processes 31 (2017): 4639–4646.

Gerrits, A. M. J., & Savenije, H. H. G. (2011). Interception. In W. Peter (Ed.), Treatise on Water Science (pp.89-101). Oxford: Academic Press. https://doi.org/10.1016/B978-0-444-53199-5.00029-4

Herwitz, S. R.: Interception storage capacities of tropical rainforest canopy trees, Journal of Hydrology, 77, 237–252, https://doi.org/10.1016/0022-1694(85)90209-4, 1985.

Jung, M., Koirala, S., Weber, U., Ichii, K., Gans, F., Camps-Valls, G., Reichstein, M. (2019): The FLUXCOM ensemble of global land-atmosphere energy fluxes. Scientific Data, 6(1). doi:10.1038/s41597-019-0076-8

Klingel, P. and Knobloch, A. (2015), A Review of Water Balance Application in Water Supply. Journal - American Water Works Association, 107: E339-E350. https://doi-org.tudelft.idm.oclc.org/10.5942/jawwa.2015.107.0084

Liu, S., Wang, T., Kang, W. et al. Several challenges in monitoring and assessing desertification. Environ Earth Sci 73, 7561–7570 (2015). https://doi-org.tudelft.idm.oclc.org/10.1007/s12665-014-3926-x

Luxemburg, W., Lecture Notes: course Hydrologie 2017, TU Delft

Martens, B., Miralles, D.G., Lievens, H., van der Schalie, R., de Jeu, R.A.M., Fernández-Prieto, D., Beck, H.E., Dorigo, W.A., and Verhoest, N.E.C.: GLEAM v3: satellite-based land evaporation and root-zone soil moisture, Geoscientific Model Development, 10, 1903–1925, doi: 10.5194/gmd-10-1903-2017, 2017.

Mitra, S., Srivastava, P. & Lamba, J. Probabilistic assessment of projected climatological drought characteristics over the Southeast USA. *Climatic Change* **147,** 601–615 (2018). https://doi-org.tudelft.idm.oclc.org/10.1007/s10584-018-2161-y

Miralles, D.G., Holmes, T.R.H., de Jeu, R.A.M., Gash, J.H., Meesters, A.G.C.A., Dolman, A.J.: Global land-surface evaporation estimated from satellite-based observations, Hydrology and Earth System Sciences, 15, 453–469, doi: 10.5194/hess-15-453-2011, 2011.

NASA (2014, 9. April). MODIS LAND PRODUCT. modis.gsfc.nasa.gov. https://mdis.gsfc.nasa.gov/data/dataprod/mod12.php

Nijzink, R., Hutton, C., Pechlivanidis, I., Capell, R., Arheimer, B., Freer, J., Han, D., Wagener, T., McGuire, K., Savenije, H., and Hrachowitz, M.: The evolution of root-zone moisture capacities after deforestation: a step towards hydrological predictions under change?, Hydrol. Earth Syst. Sci., 20, 4775–4799, https://doi.org/10.5194/hess-20-4775-2016, 2016.

Pastorello, G., Trotta, C., Canfora, E. et al. (2020): The FLUXNET2015 dataset and the ONEFlux processing pipeline for eddy covariance data. Sci Data 7, 225 (2020). https://doi.org/10.1038/s41597-020-0534-3 [.bib, .ris] Retrieved: 19.11.2020

Porporato, A.,Laio, F.;Ridolfi,L.,Rodriguez-Iturbe,I.,: Plants in water-controlled ecosystems: active role in hydrologic processes and response to water stress: III. Vegetation water stress, (2001) Water Ressources https://doi.org/10.1016/S0309-1708(01)00006-9

Ryu, Y., et al. (2011), Integration of MODIS land and atmosphere products with a coupled-process model to estimate gross primary productivity and evapotranspiration from 1 km to global scales, Global Biogeochem. Cycles,25, GB4017, doi:10.1029/2011GB004053

Steudle E., Water uptake by roots: effects of water deficit, Journal of Experimental Botany, Volume 51, Issue 350, September 2000, Pages 1531–1542, https://doi-org.tudelft.idm.oclc.org/10.1093/jexbot/51.350.1531

Sung, L. (2017), Effect of Hydrological Cycle on Climate. International Journal For Empirical Education and Research, 1(2), 18-27.

Ullah, Waheed & Wang, Guojie & Ali, Gohar & Hagan, Daniel & Bhatti, Asher & Lou, Dan. (2018). Comparing Multiple Precipitation Products against In-Situ Observations over Different Climate Regions of Pakistan. Remote Sensing. 11. 10.3390/rs11060628. [Accessed 03 June 2021].

Vera, J. Vera, I. Abrisqueta, I. Abrisqueta, W. Conejero, W. Conejero, & M. C. Ruiz-Sanchez, M. C. Ruiz-Sanchez. (2017). Precise sustainable irrigation: a review of soil-plant-atmosphere monitoring. Acta horticulturae, 195-202. doi: 10.17660/Acta-Hortic.2017.1150.28

Viovy, N. 2018. CRUNCEP Version 7 - Atmospheric Forcing Data for the Community Land Model. Research Data Archive at the National Center for Atmospheric Research, Computational and Information Systems Laboratory. https://doi.org/10.5065/PZ8F-F017. [Accessed 03 June 2021].

Wang-Erlandsson, L., Bastiaanssen, W. G. M., Gao, H., Jägermeyr, J., Senay, G. B., van Dijk, A. I. J. M., Guerschman, J. P., Keys, P. W., Gordon, L. J., and Savenije, H. H. G.: Global root zone storage capacity from satellite-based evaporation, Hydrol. Earth Syst. Sci., 20, 1459–1481, https://doi.org/10.5194/hess-20-1459-2016, 2016. Retrieved: 19.11.2020

Xu, CY., Singh, V.P. A Review on Monthly Water Balance Models for Water Resources Investigations. Water Resources Management 12, 20–50 (1998). https://doi-org.tudelft.idm.oclc.org/10.1023/A:1007916816469

Ying Fan, Gonzalo Miguez-Macho, Esteban G. Jobbágy, Robert B. Jackson, Carlos Otero-Casal, Hydrologic regulation of plant rooting depth, Proceedings of the National Academy of Sciences

# Appendix

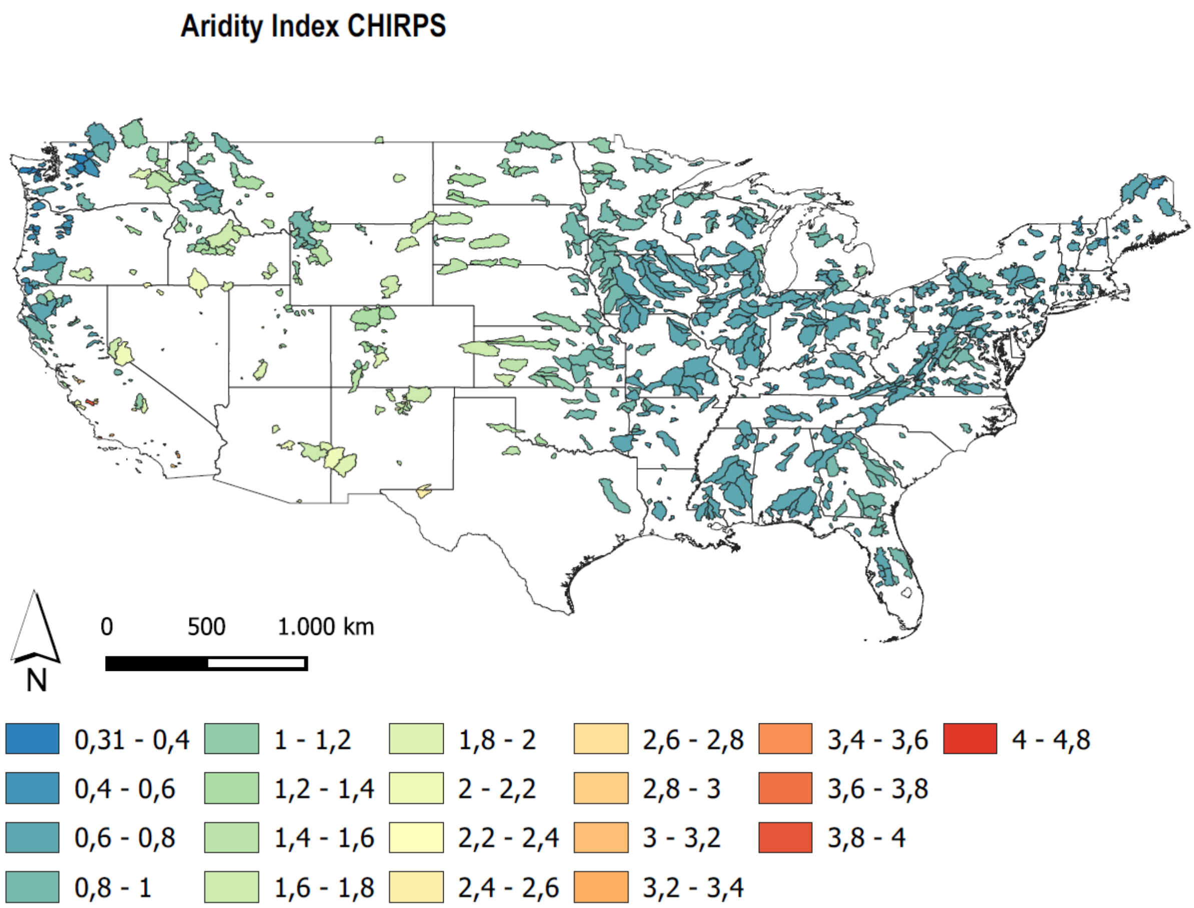


Figure 30: Average aridity index (-) in the selected U.S. watersheds for the period 2001-2016, based on annual aridity indices. Precipitation was derived from the CHIRPS dataset and potential evaporation from the GLEAM dataset.

$$D_{avg} = \frac{\overline{E_{pot}}}{\overline{P}} \tag{17}$$

As indicated in equation 17, the aridity index is defined as the ratio between long-term potential evaporation and long-term precipitation (Luxembourg, 2017). Potential evaporation corresponds to the amount of water that leaves the watershed vertically due to available solar energy. Precipitation corresponds to the amount of water supplied vertically to the catchment in the form of rain. An aridity index greater than 1 therefore corresponds to an area where more water is lost vertically than is supplied by precipitation and therefore is defined as an arid area. Catchments with an aridity index of less than 1 are defined as humid.

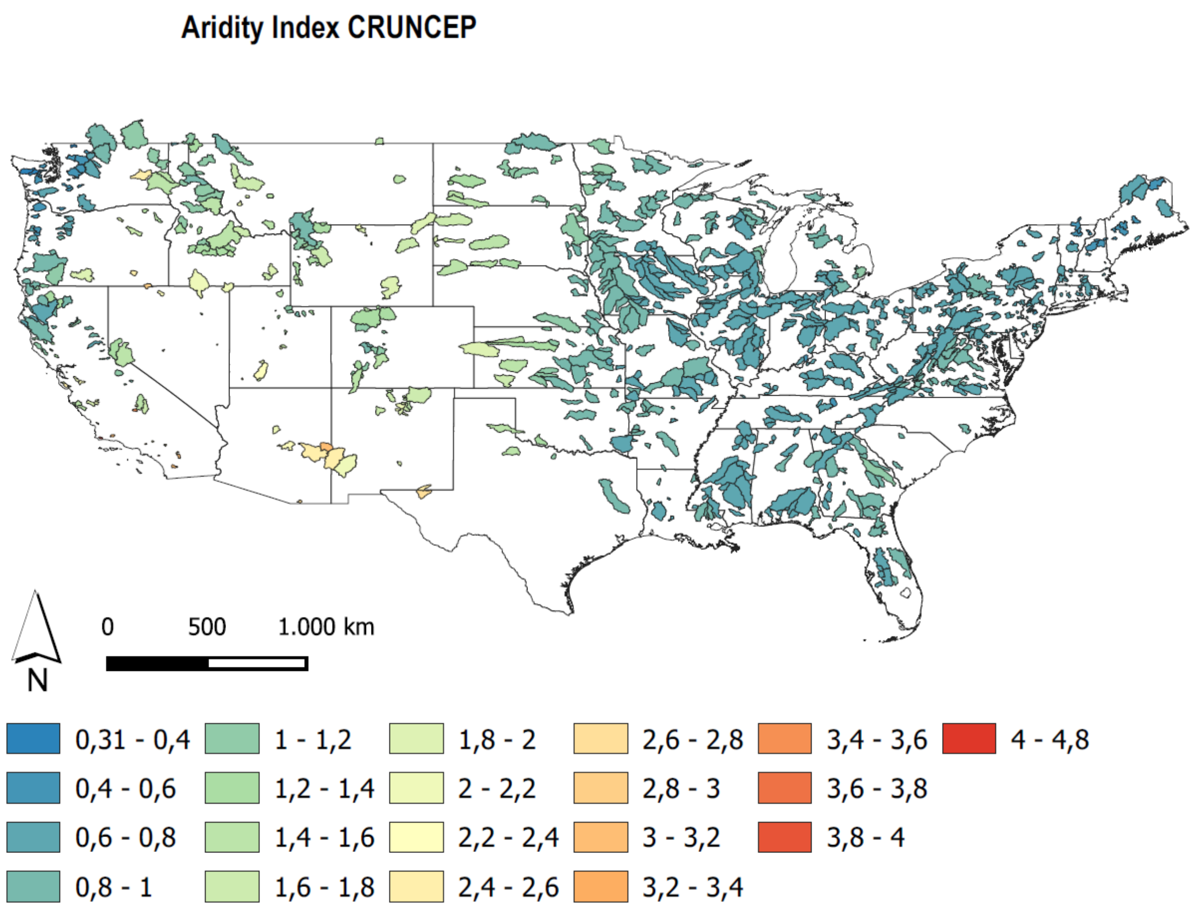


Figure 31: Average aridity index (-) in the selected U.S. watersheds for the period 2001-2016, based on annual aridity indices. Precipitation was derived from the CRUNCEP dataset and potential evaporation from the GLEAM dataset.

The dryness indices and their positions shown in Figure 31 are very similar to those calculated from the CHIRPS data. As with the CHIRPS data, the respective dryness indices can be matched with the correlations of the respective trends in root spear deficits. These are shown in Figure 31 and Figure 32. As with the CHIRPS data, the correlations increase with increasing moisture. Thus, a dependence of the root storage deficit on the precipitation supply can be demonstrated here as well.

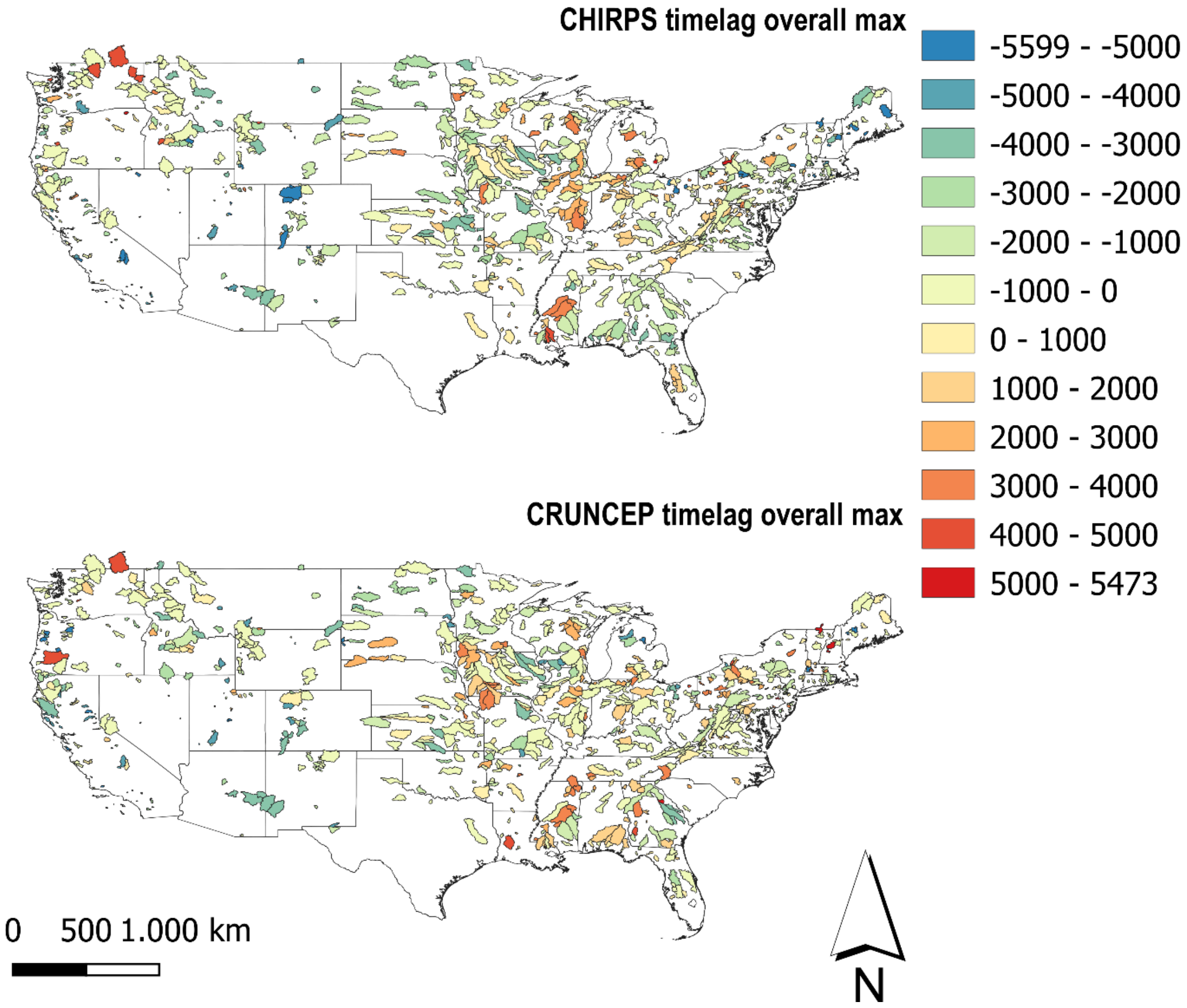


Figure 32: Visualization of time lag of the total maxima. As can be seen in the respective results there is a tendency of positive time lag meaning that the maximum derived with the Discharge method has occurred before the maximum derived from the FLUXCOM method.

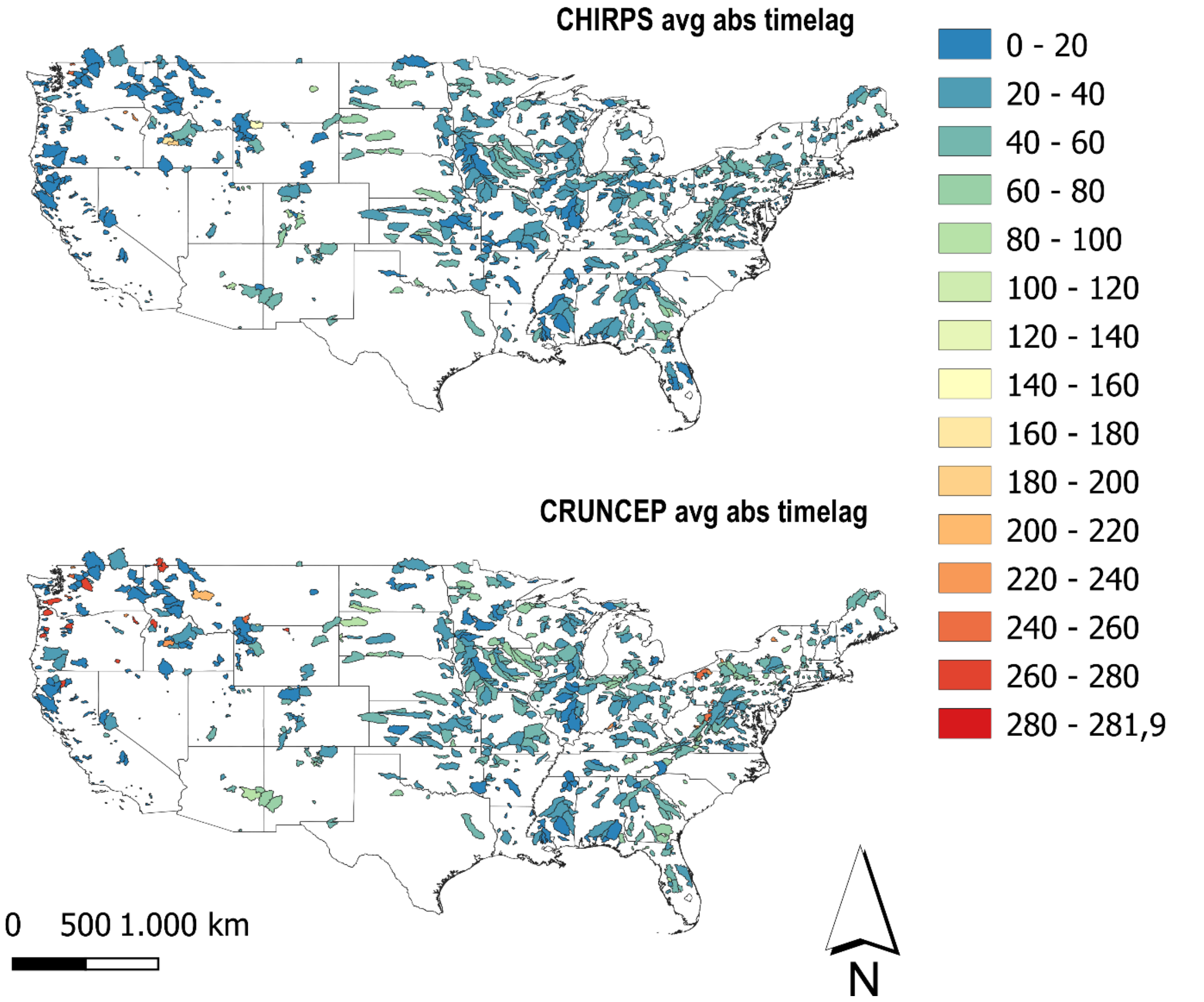


Figure 33: Average annual absolute time lag for both precipitation datasets. As can be seen in both figures the average annual time lag in respective maximum rarely exceeds 120 days. Whether the FLUXCOM method result implies earlier maxima than the Discharge method can not be derived from this Figure.

### Catchment areas not meeting boundary conditions

In other areas, however, the results determined on the basis of the calculation shown are clearly flawed: as can be seen in Figure 34, the results lead to contradictory outcomes. The root storage deficit calculated with the Discharge method is consistently zero, which can be explained by the fact that the incoming precipitation minus the local Discharge leaves no more room for additional transpiration. This means that the calculated coefficients are negative and thus the water balance is already closed without transpiration. In contrast to the FLUXCOM transpiration $E_{tr_{FL}}$, the iteratively determined transpirations $E_{tr_0}$ and $E_{tr_i}$ are permanently equal to zero. This is also supported by the fact that the discharge (mm/d) is disproportionately high. A possible explanation would be the incorrect allocation of the discharge to the catchment area. Alternatively, the deficits suggested only by the FLUXCOM dataset could also be the result of groundwater extraction.

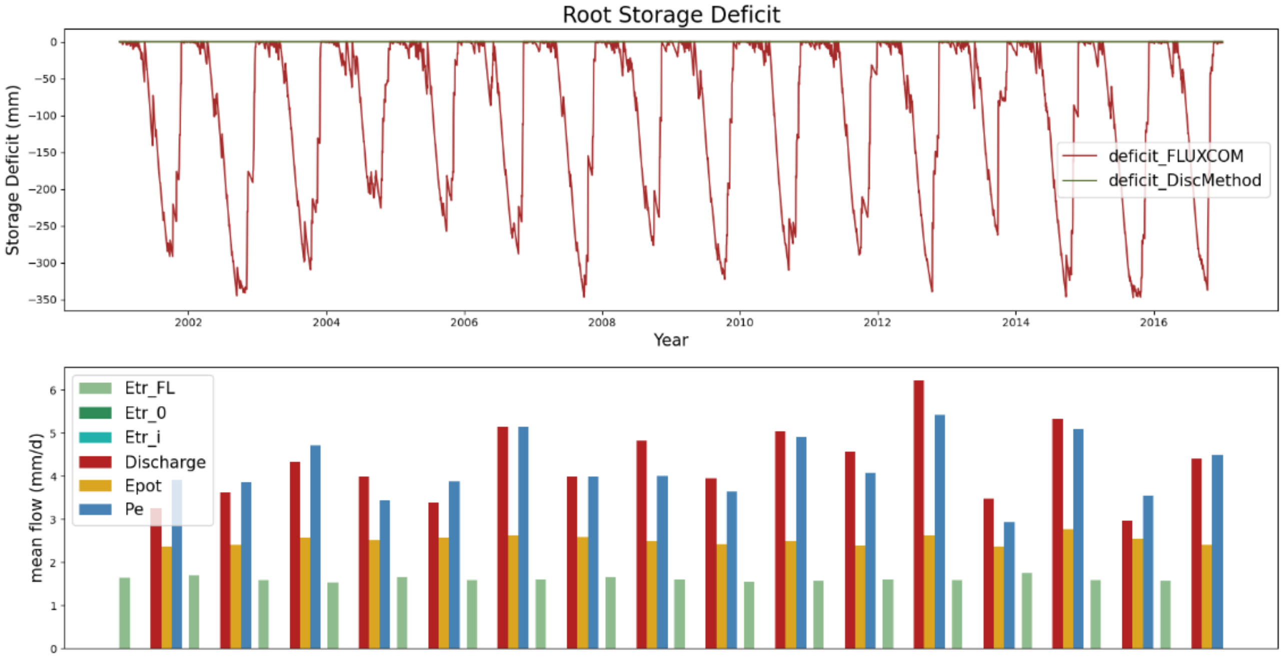


Figure 34: Illustration of root storage deficit (mm) on the South Santiam River below Cascadia OR (14185000), derived from the CHIRPS dataset including annually used mean values.

In Figure 35, however, the root storage deficit continues to develop towards negative infinity, which is consistent with the fact that FLUXCOM transpiration is permanently greater than effective precipitation. This means that for these areas the original assumption that the water cycle is not yet closed has not been met and these areas are not eligible for the actual analysis.

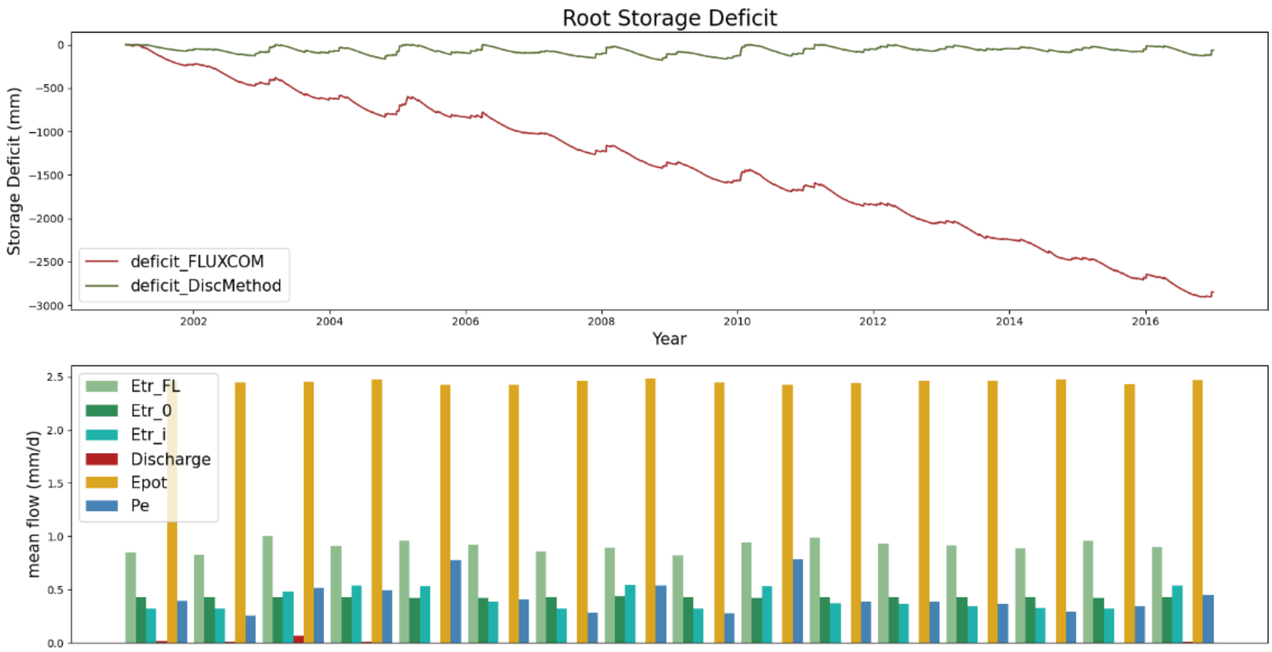


Figure 35: Illustration of root storage deficit (mm) in BORREGO PALM C NR BORREGO SPRINGS CA (10255810) derived from CHIRPS including annual mean values used.

As with the CHIRPS data, Figure 36 and Figure 37 also show comparable sets of errors. Thus, the strong dependence on the precipitation data can be invalidated, as two different data sets provide comparable results.

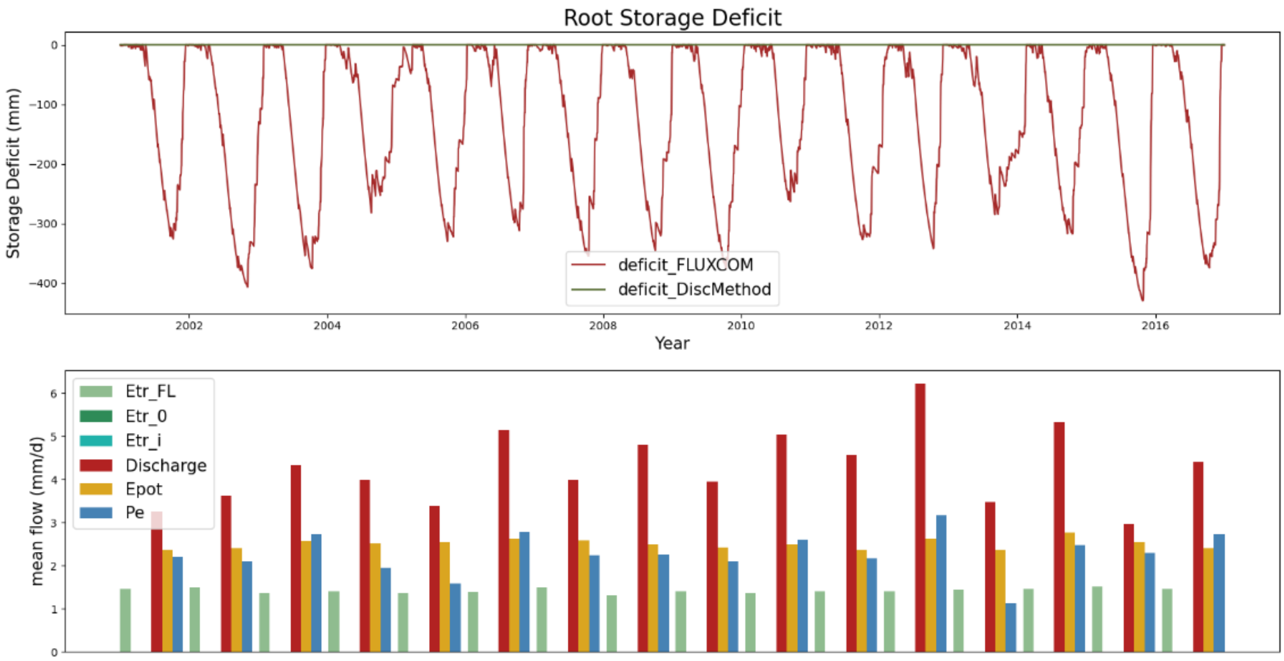


Figure 36: Illustration of root storage deficit (mm) on the South Santiam River below Cascadia, OR (14185000), derived from the CRUNCEP dataset, including visualisation of annually calculated mean forcings in (mm/day)

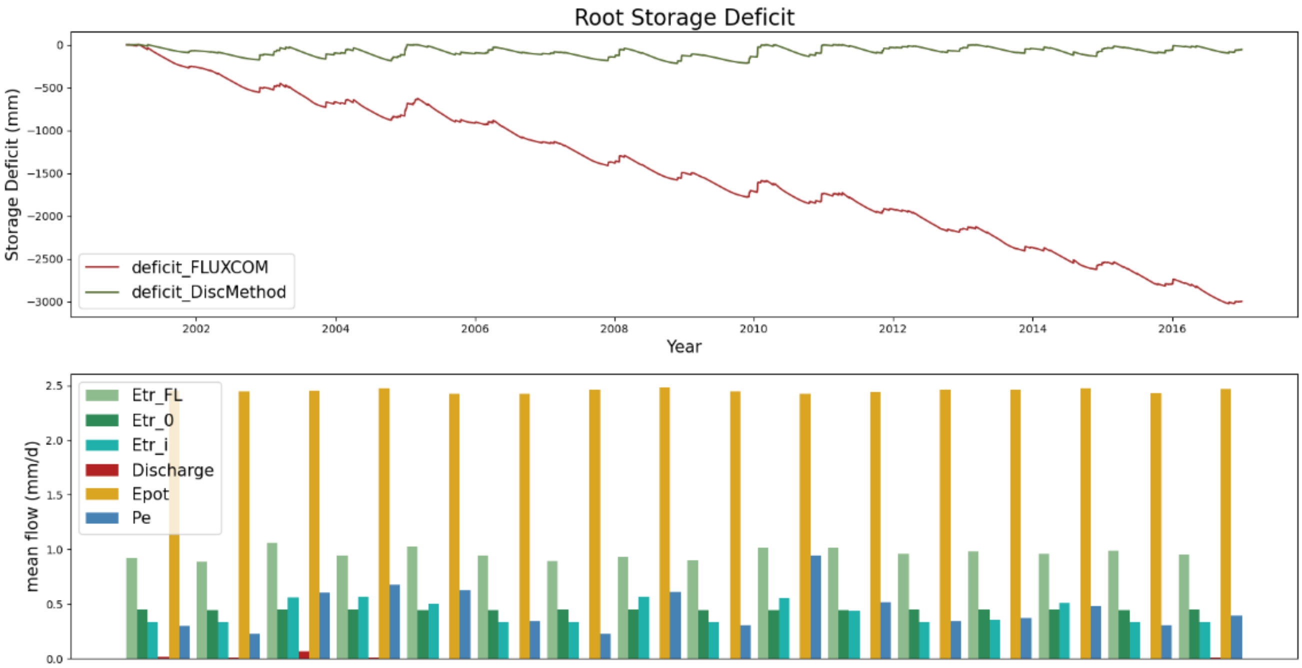


Figure 37: Illustration of root storage deficit (mm) on the Tradewater River at Borrego Palm NR Borrego Springs, CA (10255810) derived from the CRUNCEP dataset, including visualisation of annual calculated mean forcing in (mm/day).

Table 4: Average values of the respective measurement parameters in the catchment areas in which neither the framework conditions are violated nor an ever-growing deficit occurs.

| EXTRACTED CRITERION | | BIAS | | | TIME LAG | | |
|---|---|---|---|---|---|---|---|
| | | **Max** | **Min** | **Avg** | **Max** | **Min** | **Avg** |
| CHIRPS | Overall max. | 972,8 | -211,74 | 178,57 | 5473 | -5808 | -671,5 |
| | Annual max. | -977,7 | -247,3 | 126,9 | 358 | -274 | 46,7 |
| CRUNCEP | Overall max. | 925,0 | -291,0 | 211,9 | 5420 | -5799 | -669,3 |
| | Annual max. | 925,4 | -401,4 | 139,9 | 337 | -362 | -38,6 |